POTENTIAL FORMULATION FOR THE DYNAMICS OF PRESSURE SPIKING IN RESPONSE TO FLUID PERCUSSION BRAIN INJURY

by

Joshua Latka

Submitted in partial fulfillment of the requirements
for the degree of Master of Science

at

Dalhousie University
Halifax, Nova Scotia
February 2017

Table of Contents

List of Tables

List of Figures

Abstract

A mathematical description of percussive pressure events is considered. This model gives a clearer clinical understanding of how these events lead to percussion injury affecting the brain, a mechanism for traumatic brain injury. The linear model presented here utilizes shell theory in parallel with fluid mechanics to describe a percussive pressure event to the head. An analytic solution is obtained and used to simulate the interaction between the skull structure and brain tissue during a head impact. Certain patterns in the results have been observed that are in agreement with current clinical knowledge, while other new findings have been observed which may lead to a greater understanding and ability to prevent traumatic brain injuries.

List of Abbreviations and Symbols Used

E	Modulus of elasticity
$I_{n+1/2}$	Modified Bessel function of the first kind
$J_{n+1/2}$	Bessel function of the first kind
P_n	Legendre polynomial
R	Radial coordinate (Dimensionless)
U	Tangential displacement (Dimensionless)
W	Radial displacement (Dimensionless)
Φ	Fluid velocity potential (Dimensionless)
β	Bending coefficient
ν	Poisson's ratio
ω	Sound speed ratio
$\overline{\Phi}$	Laplace transformed fluid velocity potential
$\underset{\sim}{\bar{p}}_0$	Pressure scale (Dimensional)
ϕ	Fluid velocity potential (Dimensional)
ρ	Density
τ	Time (Dimensionless)
θ	Elevation angle
$\underset{\sim}{P}_0$	External pressure (Dimensionless)
$\underset{\sim}{P}_a$	Total Pressure (Dimensionless)

p_0	External pressure (Dimensional)
p_a	Total pressure (Dimensional)
c_f	Speed of sound in the fluid (Dimensional)
c_p	Speed of sound in the shell (Dimensional)
h	Skull thickness (Dimensional)
$i_{n+1/2}$	Modified spherical Bessel function of the first kind
$j_{n+1/2}$	Spherical Bessel function of the first kind
n	Modal integer
r	Radial coordinate (Dimensional)
r_0	Radius of the shell
t	Time (Dimensional)
t_c	Impact contact time (Dimensional)
u	Tangential displacement (Dimensional)
w	Radial displacement (Dimensional)
w_0	Displacement Scale

Acknowledgements

I would like to thank my supervisors Dr. Guy Kember and Dr. Serguei Iakovlev of the Engineering Mathematics and Internetworking Department at Dalhousie University for their guidance and wisdom throughout this project. Their immense passion for this research is clear to all involved and without them this project would not have been possible. Also, thank you to my committee member, a medical professional, and clinical liaison, Dr. Sultan Darvesh for his knowledge and support that have been invaluable. As well, thank you to my other committee member Dr. Gordon Fenton for his advice and timely input into this work. Finally, the tireless work of student Greg d'Eon stream-lined my work and made completion of my research much easier; thank you.

Chapter 1

Introduction

Over the last decade concussions, or more precisely traumatic brain injuries (TBI), have entered the spotlight as a frequent and devastating form of brain injury. Traumatic brain injury is one of the leading causes of morbidity and mortality at all ages. Disruption of brain tissues during such a head impact leads to a number of clinical effects including concussion. These events consist of an external force to the head, either from a physical blunt force trauma or a blast pressure wave. Depending on the type of brain injury (blast/blunt), two main mechanisms leading to brain damage have been proposed. These are inertial, or viscous, events resulting from the rotation and shearing of the brain, and percussive pressure events resulting in pressure gradients and compression of the brain. Injuries resulting from these events can result in various clinical effects from the mild inconvenience of a headache lasting several days to the onset of progressive degenerative disease of the brain, known as chronic traumatic encephalopathy (CTE) (Gavett et al., 2011; McKee et al., 2016). These effects are well-known and documented through recent studies (Guskiewicz et al., 2005; McKee et al., 2009; Omalu et al., 2005). In response to these studies, the severity of concussions has been acknowledged within areas such as professional sports (Viano et al., 2005) through the implementation of new rules and regulations regarding concussions (Aubry et al., 2002; Bonds et al., 2014; Cantu, 1992) With this being said, there remains a distinct lack of understanding on what is occurring within the brain during an impact (Gupta and Przekwas, 2013).

In order to reliably prevent concussions and brain injuries, it is necessary to not only study the after-effects of a concussion but also to gain an understanding of what happens in the brain during an impact. This includes pressure gradients and inertial effects associated with large stresses and strains within the brain before, during, and after an impact and the physiological response of the brain to impact. With the recent rise in focus on concussions, especially in sports and the military, many studies have

tried to 'solve' the concussion problem (Bolouri and Zetterberg, 2015; Thompson et al., 2005; Wei et al., 1981). There are a number of studies using animal models and theoretical models of various kinds that focus, for example, on a 'better helmet' or a consistent way of mimicking features of TBI (Bar-Kochba et al., 2012). These studies have been very useful to uncover the complexity of the brain's response to sudden impacts both large and small. As a result, the definition of concussion has moved from the standard catastrophic event of being 'knocked out' to a spectrum where long-term exposure of the brain to a low-impact environment, such as repeated and frequent injury in sports, leads to serious and permanent long-term brain damage (Ommaya and Gennarelli, 1974).

Studies related to traumatic brain injuries so far have been categorized into two broad groups: clinical and theoretical. Clinical studies focus on experimental techniques such as an animal models where brain scans are taken before and after an impact is delivered to an anaesthetized live or dead animal (Flierl et al., 2009; Marmarou et al., 1994; Foda and Marmarou, 1994; Kabadi et al., 2010). In others, accelerometers are mounted on helmets worn by people or test dummies and gross measurements of accelerations are taken (Guskiewicz and Mihalik, 2011; Duma et al., 2005). When the helmets are worn by people, the impact effect upon function is also noted (Council, 2014). As for the theoretical studies, these focus on creating computer models of the brain and subjecting the model to impacts and approximating the equation solution using numerical methods such as finite element analysis (Cloots et al., 2010; Takhounts et al., 2003). These models range in complexity and their main strength is the capacity to include many factors within the brain structure such as axon orientation and location of blood vessels and test the effects of these features in ways that cannot be entertained in the clinical setting.

Initial studies of concussion, both theoretical and clinical, have tended to take in the broader context of the problem (Ommaya and Gennarelli, 1974; Engin, 1969). These were quickly followed by those with a more targeted focus once the complexity of concussion injury began to become apparent. For example, there are studies that have focused only on inertial collisions, or viscous events, associated with the rotation of the head(Stevenson, 2006). These types of injuries are common during a blunt impact to the head or resulting from head trauma commonly associated with most

car accidents. Others have considered purely percussive (non-inertial, non-rotational) events that are more common in the military such as explosions and blast waves (Moore et al., 2009; Thibault et al., 1992). While there is plenty of research regarding these percussive events there is little knowledge of the extent to which percussive events cause and/or interact with inertial aspects of concussion.

A key finding in the area of concussion has been the relevance of linear acceleration that occurs in rapid pressure events versus rotational acceleration experienced, for example, in glancing blows. While there is a reasonable understanding of linear acceleration and its related injury thresholds (Zhang et al., 2004), these do not seem to produce concussions experimentally and that observation has led to a deeper study of rotational acceleration (Meaney and Smith, 2011; Zhang et al., 2006). It is often pointed out that shear deformation caused by rotational acceleration is the predominant mechanism of concussive injuries due to the higher resistance of the brain to compression (pressure events) than to shear (rotational events) (Bradshaw and Morfey, 2001). However, when linear acceleration is coupled with minor shear effects, concussion is observed experimentally (Frost, 2011) and this points out that there is a need for more basic understanding of the underlying physics of concussion than is already available.

As explained above, it is clear that there are many unknowns in the concussion problem. A notable, and intensively studied example is diffuse axonal injury (DAI). DAI is one of the most common and devastating types of TBI leading to unconsciousness and coma, yet no theoretical model has been able to reproduce even the basic features of DAI. Multi-scale finite element models have accounted for immense detail in the brain structure, such as axon orientation and the wrapping around of blood vessels in the search to find structures that may exacerbate shear effects, without success (Cloots et al., 2010; Miller et al., 1998). The only conclusion that can be garnered from this is that even in acute injury such as DAI there are mechanisms of interaction between the global and microscopic levels within the brain that are yet to be discovered (Smith et al., 2003). Unravelling these will require the modelling of the coupling of physical effects such as pressure and inertial influences with the response of microscopic structures within the brain.

The aforementioned studies have led to some general conclusions surrounding

linear and rotational accelerations along with qualitative descriptions of CTE and DAI. However, their most important discovery has been the level of complexity in the response of a sophisticated and delicate organ like the brain to impact injuries. This complexity, while not surprising in hindsight, is an interesting example of the need to build theories that mix biology and engineering in novel ways (Goldsmith, 2001; Goldsmith and Monson, 2005). A starting point may be to rethink previous understanding of basic models (Engin, 1969; Chan and Liu, 1974) and repackage the mathematical description of percussion injury and concussion in a way that is more clinically and pathologically useful (Choe, 2016). Hence, the goal of this thesis is to develop a mathematical description of percussive pressure events that gives a clearer clinical understanding of how percussion injury affects the brain.

Chapter 2

Mathematical Model

2.1 The Potential Formulation

We consider a fluid-filled spherical shell of radius r_0 and thickness h. The physical representation of this model can be seen in Figure 2.1 with the skull and brain being represented by the shell and fluid respectively. It is known that $h/r_0 \gg 1$ and also that the shell deflections are small in comparison to its thickness. It follows from this knowledge that linear shell theory is applicable. The tangential and radial displacements of the shell are u and w respectively as seen in Figure 2.2. The shell material is defined by density ρ_p, sound speed c_p, Poisson's ratio ν, and modulus of elasticity E. The fluid is defined by density ρ_f, and sound speed c_f. The shell is subjected to a direct impact resulting in an incident pressure $\underset{\sim}{p}_0$.

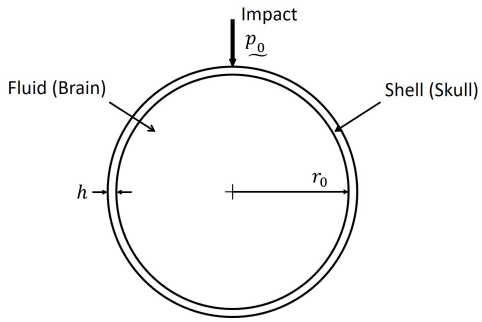

Figure 2.1: Model Description

2.2 Dimensional Form

The full problem is stated in dimensional form with all boundary and initial conditions.

The potential equation in spherical coordinates is satisfied by the fluid,

$$\phi_{rr} + \frac{2}{r}\phi_r + \frac{1}{r^2}\phi_{\theta\theta} + \frac{\cot(\theta)}{r^2}\phi_\theta = \frac{1}{c_f^2}\phi_{tt} \ , \tag{2.1}$$

with elevation angle θ and the radius is r. A subscript notation has been used for greater readability to denote partial derivatives so that $\dfrac{\partial^2 y}{\partial x^2}$ is written as y_{xx}. The azimuthal dependence of the potential is neglected since the external forcing to the shell will be assumed to have azimuthal symmetry.

There are two boundary conditions that relate the fluid to its shell enclosure at $r = r_0$. The first is that the normal velocity of the shell and fluid in the radial direction must be equal,

$$\phi_r = -w_t, \qquad r = r_0 \ . \tag{2.2}$$

This condition in (2.2) is consistent with the acceleration of the fluid and shell being equal because $\phi_t(\theta, r, t) = p(\theta, r, t)$ and differentiating 2.2 with respect to time yields the radial acceleration of the shell which is proportional to the pressure gradient (at the shell this has only a radial component).

The fluid potential satisfies zero initial conditions

$$\phi = 0 \quad \phi_t = 0 \quad \text{at} \quad t = 0 \ .$$

The second condition relates to conservation of energy and the satisfaction by the displacements of a minimal energy principle (Junger and Feit, 2003). The shell, under the assumption of azimuthal symmetry assumed here, is allowed to deform in the radial direction as $w(\theta, t)$ and tangentially oriented with change in elevation variable θ as $u(\theta, t)$. The coordinate system in use can be see in Figure 2.2.

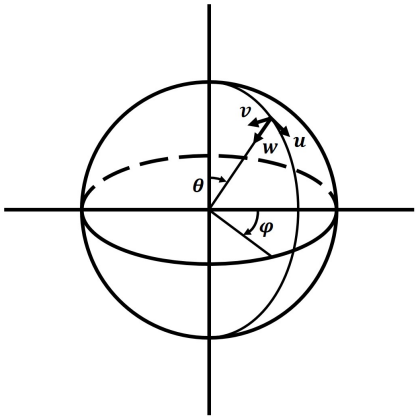

Figure 2.2: Spherical coordinate system

The displacements $u(\theta,t)$ and $w(\theta,t)$ satisfy the coupled system of equations (Junger and Feit, 2003)

$$(1+\beta^2)\left[u_{\theta\theta}+\cot(\theta)u_\theta-(\nu+\cot^2(\theta))u\right]u+\beta^2 w_{\theta\theta\theta}+\beta^2\cot(\theta)w_{\theta\theta}- \left[(1+\nu)+\beta^2(\nu+\cot^2(\theta))\right]w_\theta=\frac{a^2}{c_p^2}u_{tt}\ , \tag{2.3}$$

and

$$\beta^2 u_{\theta\theta\theta}+2\beta^2\cot(\theta)u_{\theta\theta}-\left[(1+\nu)(1+\beta^2)+\beta^2\cot^2(\theta)\right]u_\theta+ \cot(\theta)\left[(2-\nu+\cot^2(\theta))\beta^2-(1+\nu)\right]u+\beta^2 w_{\theta\theta\theta\theta}+2\beta^2\cot(\theta)w_{\theta\theta\theta}- \beta^2(1+\nu+\cot^2(\theta))w_{\theta\theta}+\beta^2\cot(\theta)(2-\nu+\cot^2(\theta))w_\theta+2(1+\nu)w +\frac{a^2}{c_p^2}w_{tt}=-\underset{\sim}{p}_a(t)\frac{(1-\nu^2)a^2}{Eh}\ , \tag{2.4}$$

and satisfy zero displacement and zero velocity initial conditions

$$\begin{aligned} u&=0, \quad t=0\\ u_t&=0, \quad t=0\\ w&=0, \quad t=0\\ w_t&=0, \quad t=0 \end{aligned} \tag{2.5}$$

The total pressure can be defined as

$$\underset{\sim}{p}_a(t)=\rho_f\phi_t+\underset{\sim}{p}_0(t)\ , \tag{2.6}$$

where ρ_f is the fluid density and $\rho_f\phi_t$ is the fluid feedback pressure. The second term, $\underset{\sim}{p}_0$, is the external pressure

$$\underset{\sim}{p}_0(t)=f(\theta)\bar{\underset{\sim}{p}}_0 e^{-t/t_c}\ , \tag{2.7}$$

where $\bar{\underset{\sim}{p}}_0$ is the pressure scale, t_c is the impact contact time, and is dependent on a function of θ, $f(\theta)$.

2.3 Physical Parameters

Many parameters within this model can be defined using physical and known values. For instance a typical boxing punch has a contact time, t_c, of approximately 0.01

seconds and an incident pressure, $\bar{\underset{\sim}{p}}_0$, of between 1 and 2 MPa. Table 2.1 summarizes this along with other physical parameters used in this model.

Parameter	Value
$\rho_{brain} = \rho_f$	1050 kg/m^3
$\rho_{skull} = \rho_p$	1750 kg/m^3
t_c	0.01 s
$\bar{\underset{\sim}{p}}_0$	1×10^6 kg/m $\cdot$ s
E_{skull}	$1.4 \times 10^(10)$ kg/m $\cdot$ s^2
r_0	0.1 m
h_{skull}	0.01 m
ν_{skull}	0.5
c_p $(skull)$	4080 m/s
c_f $(brain)$	1500 m/s

Table 2.1: Physical Parameters

2.4 Rescaling

In order to expose the parametric dependence of the model equations and thus gain an understanding of the physics represented by the model, a rescaling was performed as indicated in Table 2.2.

Parameter	Definition
τ	$\frac{c_f t}{r_0}$
R	$\frac{r}{r_0}$
$\Phi(R,\theta,\tau)$	$\frac{\phi(r,\theta,t)}{\phi_0}$
$U(\theta,\tau)$	$\frac{u(\theta,t)}{w_0}$
$W(\theta,\tau)$	$\frac{w(\theta,t)}{w_0}$
$\underline{P}_a(\tau)$	$\frac{\underline{p}_a(t)}{\bar{\underline{p}}_0}$
$\underline{P}_0(\tau)$	$\frac{\underline{p}_0(t)}{\bar{\underline{p}}_0}$
ω	$\frac{c_p}{c_f}$

Table 2.2: Rescaled dependent and independent variables.

These rescaled variables in Table 2.2 resulted in a set of dimensionless parameter groupings that define the parametric dependence of the solution. The three groupings that appear within this dimensionless form are carried throughout the problem and are of particular physical interest

1. The shell velocity 'feed forward' parameter, b, relates to the continuity of acceleration at the shell-fluid interface in equation (2.2). The term 'feed forward' means here that the external pressure 'causes' the shell movement and this movement results in an 'effect' on the fluid at interface between the two. This dimensionless parameter is

$$b = \left(\frac{w_0}{\phi_0}\right) c_f \ . \tag{2.8}$$

2. The 'feed back' of fluid pressure a is in response to the external pressure that initiated a movement of the shell and led to a reaction of the fluid. This term is represented in the model on the right-hand-side of the radial displacement shell equation in equation (A.2). In equation (2.6) $\rho_f \phi_t$ appears and rescaling of equation (2.6) leads to

$$a = \left(\frac{\phi_0}{\underset{\sim}{\bar{p}}_0}\right) \left(\frac{\rho_f c_f}{r_0}\right) \ . \tag{2.9}$$

3. Finally, defining the dimensionless group

$$c = \left(\frac{(1-\nu^2)\underset{\sim}{\bar{p}}_0}{E}\right) \left(\frac{r_0}{w_0}\right) \left(\frac{r_0}{h}\right) \tag{2.10}$$

and scaling it by $\omega^2 = (c_p/c_f)^2$ arising from the right-hand-side of the radial displacement shell equation in (A.2) leads to the definition

$$\tilde{c} = c\omega^2 \ . \tag{2.11}$$

The parameter $\tilde{c}$ represents the product of four things: (i) the relative size of the impact pressure $\underset{\sim}{\bar{p}}_0$ relative to a 'shell' pressure involving E and ν, (ii) the radius r_0 to shell thickness h, (iii) the radius r_0 to the displacement scale w_0 and (iv) the relative size of the wave speed in the fluid to the wave speed in the shell.

Even without access to the final solution, it can be seen here that the solution dynamics are independent of the scales ϕ_0, w_0 and $\underset{\sim}{\bar{p}}_0$. In fact, the solution and its dynamics depend upon one parameter: the product $a \cdot b \cdot \tilde{c}$. This is due to the neglecting of viscosity in the mathematical model. Stated another way, in the absence of viscosity, this mathematical model represents an approximation where the size of the pressure, the displacement, and the impact pressure are neglected in determining

the shell-fluid dynamics. This can again be seen later on when the model solution is discussed.

To connect the model to the concussion application, it is useful to explicitly state those parts of the dimensionless parameters that are known and they are

Parameter	Subparameter Definition	Subparameter Value
a	$\left(\frac{\phi_0}{\bar{p}_0}\right) a_m$	$a_m = \frac{\rho_f c_f}{r_0} = 1.58 \times 10^7$
b	$\left(\frac{w_0}{\phi_0}\right) b_m$	$b_m = c_f = 1500$
c	$\left(\frac{\bar{p}_0}{w_0}\right) c_m$	$c_m = \frac{(1-\nu^2) r_0^2}{Eh} = 5.4 \times 10^{-11}$
$\tilde{c}$	$\left(\frac{\bar{p}_0}{w_0}\right) \tilde{c}_m$	$\tilde{c}_m = \left[\frac{(1-\nu^2) r_0^2}{Eh}\right] \omega^2 = 4 \times 10^{-10}$

Table 2.3: Dimensionless Groupings and Parameters

where $\omega = c_p/c_f = 2.72$ from Table 2.2.

The product $a \cdot b \cdot \tilde{c} = (\rho_f c_f^2 (1-\nu^2) r_0)/(Eh)\omega^2 = \mathcal{O}(10)$ is the central parameter that determines the shell-fluid dynamical interaction as approximated by the mathematical model considered here. The fact this parameter is large compared to unity comes from the head injury model where the skull is considerably more rigid than the brain tissue.

2.5 Dimensionless Problem

Nondimensionalizing equation (2.1) using Table 2.2 gives

$$\Phi_{RR} + \frac{2}{R}\Phi_R + \frac{1}{R^2}\Phi_{\theta\theta} + \frac{\cot(\theta)}{R^2}\Phi_\theta = \Phi_{\tau\tau} \ . \tag{2.12}$$

The initial conditions are all zero for the potential Φ and shell displacements U

and W along with the derivatives with respect to time so that

$$\begin{aligned} \Phi = 0, \quad \Phi_\tau = 0, \quad \tau = 0 \\ U = 0, \quad U_\tau = 0, \quad \tau = 0 \\ W = 0, \quad W_\tau = 0, \quad \tau = 0 \end{aligned} \tag{2.13}$$

At the shell-fluid interface the velocity is continuous so that

$$\Phi_R = -bW_\tau \ \text{ at } R = 1 \ . \tag{2.14}$$

The dimensionless shell equations are

$$\begin{aligned} (1+\beta^2)\omega^2 U_{\theta\theta} + (1+\beta^2)\omega^2 \cot(\theta) U_\theta - (1+\beta^2)\omega^2(\nu + \cot^2(\theta))U - \beta^2\omega^2 W_{\theta\theta\theta} \\ -\beta^2\omega^2 \cot(\theta) W_{\theta\theta} + \left[1 + \nu + \beta^2\left(\nu + \cot^2(\theta)\right)\right]\omega^2 W_\theta \\ -U_{tt} = 0 \ , \end{aligned} \tag{2.15}$$

and

$$\begin{aligned} \beta^2\omega^2 U_{\theta\theta\theta} + 2\beta^2\omega^2 \cot(\theta) U_{\theta\theta} - \left[(1+\nu)(1+\beta^2) + \beta^2 \cot^2(\theta)\right]\omega^2 U_\theta \\ + \cot(\theta)\left[(2 - \nu + \cot^2(\theta))\beta^2 - (1+\nu)\right]\omega^2 U \\ -\beta^2\omega^2 W_{\theta\theta\theta\theta} - 2\beta^2 \cot(\theta)\omega^2 W_{\theta\theta\theta} + \beta^2(1 + \nu + \cot(\theta)^2)\omega^2 W_{\theta\theta} \\ -\beta^2 \cot(\theta)(2 - \nu + \cot(\theta)^2)\omega^2 W_\theta - 2(1+\nu)\omega^2 W \\ -W_{\tau\tau} = -\tilde{c}\underset{\sim}{P}_a(\tau) \ . \end{aligned} \tag{2.16}$$

The total pressure is now

$$\underset{\sim}{P}_a(\tau) = a\Phi_\tau + \underset{\sim}{P}_0(\tau) \ , \tag{2.17}$$

where a is defined by equation (2.9). The external pressure, $\underset{\sim}{P}_0$, is the dimensionless form

$$\underset{\sim}{P}_0(\tau) = f(\theta)e^{-\tau/\tilde{\beta}} \ , \tag{2.18}$$

where $\tilde{\beta}$ is the relative size of the impact time scale relative to the fluid potential time scale $r_0/(c_f t_c)$. Referring to Table 2.2

$$\tilde{\beta} = \frac{t_c c_f}{r_0} = 150 \gg 1 \ . \tag{2.19}$$

The size of this parameter illustrates the wide gap between the time scale over which the impact occurs compared with the rate that its initial effect passes through the shell and fluid. In other words, the initial effect can be seen passing through the fluid numerous times before the entire impact is complete. A first approximation will be to consider the impact as constant given $\tau \ll \tilde{\beta}$.

2.6 Laplace Transform Solution of Dimensionless Problem

2.6.1 Laplace Transform of Wave Equation

The dimensionless form of the wave equation (2.12) is

$$\Phi_{RR} + \frac{2}{R}\Phi_R + \frac{1}{R^2}\Phi_{\theta\theta} + \frac{\cot\theta}{R^2}\Phi_\theta = \Phi_{\tau\tau} \ . \tag{2.20}$$

We apply Laplace transform with respect to τ to (2.20) to arrive at

$$\overline{\Phi}_{RR} + \frac{2}{R}\overline{\Phi}_R + \frac{1}{R^2}\overline{\Phi}_{\theta\theta} + \frac{\cot\theta}{R^2}\overline{\Phi}_\theta = s^2\overline{\Phi} \ , \tag{2.21}$$

where $\overline{\Phi}(R, s, \theta)$ denotes the Laplace transform of $\Phi(R, \tau, \theta)$ (From here on, an overbar denotes the Laplace transform of the variable in question).

Representing $\overline{\Phi}(R, s, \theta)$ as a generic separated product of $Q(R, s)$ and $P(\theta)$ yields

$$\overline{\Phi}(R, \theta, s) \propto Q(R, s)P(\theta) \ , \tag{2.22}$$

where the $\propto$ refers to fact that any function of the Laplace transform variable s that represents a constant multiple in equation (2.22) is also a solution. With this definition, equation (2.20) becomes

$$\frac{R^2Q_{RR} + 2RQ_R - R^2s^2Q}{Q} + \frac{P_{\theta\theta} + \cot\theta P_\theta}{P} = 0 \ . \tag{2.23}$$

$P(\theta)$ satisfies the Legendre equation

$$P_{\theta\theta} + \cot\theta P_\theta - n(n+1)P = 0 \ , \tag{2.24}$$

where $n(n+1)$ is an integer to ensure that the series solution truncates and is convergent for $0 \leq \theta \leq \pi$. Given the presence of the integer n, $Q(R, s)$ is renamed to

$Q_n(R,s)$ to reflect the solution modal nature (from here on, a subscript n denotes a modal form of the variable in question). Equation (2.23) then leads to

$$R^2 Q_{nRR} + 2RQ_{nR} - (R^2 s^2 + n(n+1))Q_n = 0 \ . \tag{2.25}$$

Equation (2.24) is the modified spherical Bessel differential equation. For the solution to be bounded at $R = 0$,

$$Q_n(R,s) = \sqrt{\frac{\pi}{2Rs}} I_{n+1/2}(Rs) \ . \tag{2.26}$$

Equation (2.24) is a Legendre differential equation and its solution is an n^{th} order polynomial that may be assumed to conveniently depend upon $\cos\theta$ such that

$$P(\theta) = P_n(\cos\theta) \ . \tag{2.27}$$

Given $Q_n(r,s)$ from the above

$$\overline{\Phi}_n(R,s) = F_n(s)\sqrt{\frac{\pi}{2Rs}} I_{n+1/2}(Rs) \ , \tag{2.28}$$

and the general solution to the field equation that satisfies zero initial conditions and is bounded at $r = 0$ is

$$\overline{\Phi}(R,\theta,s) = \sum_{n=0}^{\infty} \overline{\Phi}_n(R,s) P_n(\theta) \ , \tag{2.29}$$

where $F_n(s)$ is absorbed into the definition of $\overline{\Phi}_n(R,s)$ for notational convenience. Note that equation (2.29) implies that a formal inversion gives the field variable as

$$\Phi(R,\theta,\tau) = \sum_{n=0}^{\infty} \Phi_n(R,\tau) P_n(\theta) \ . \tag{2.30}$$

2.6.2 Laplace Transform of Dimensionless Separated Shell Equations

The dimensionless shell displacements may be written in the separated form

$$\begin{aligned} W(\theta,t) &= \sum_{n=0}^{\infty} P_n(\theta) W_n(t) \\ U(\theta,t) &= -\sum_{n=0}^{\infty} P_n^1(\theta) U_n(t) \end{aligned} \tag{2.31}$$

This yields (see Appendix A for details)

$$(1+\beta^2)\omega^2\left[1-\nu-n(n+1)\right]U_n(\tau)+\left[(n(n+1)-1+\nu)\beta^2+1+\nu\right]\omega^2 W_n(\tau) \\ -U_{n\tau\tau}=0\ , \tag{2.32}$$

and

$$\omega^2\left[-(1+\nu)n(n+1)+\beta^2(1-n(n+1)-\nu)n(n+1)\right]U_n(\tau) \\ -\omega^2\beta^2 n(n+1)\left[1-n(n+1)-\nu\right]W_n(\tau) \\ +2(1+\nu)\omega^2 W_n(\tau)+W_{n\tau\tau}=-\tilde{c}\left(a\Phi_{n\tau}(R=1,\tau)+A_n\right)\ . \tag{2.33}$$

The inhomogeneous terms on the right-hand-side of equation (2.33) follow from equation (2.30) and the total pressure in equation (2.18) written as

$$\underset{\sim}{P}_0(\tau)=\sum_{n=0}^{\infty}A_n P_n(\theta)e^{-\tau/\tilde{\beta}}\ , \tag{2.34}$$

and further approximated as

$$\underset{\sim}{P}_0(\tau)=\sum_{n=0}^{\infty}A_n P_n(\theta) \tag{2.35}$$

under the assumption that $\tau \ll \tilde{\beta}=150$.

Taking Laplace transforms and applying the zero initial conditions in equation (2.13)

$$(1+\beta^2)\omega^2\left[1-\nu-n(n+1)\right]\overline{U}_n(s)+\left[(n(n+1)-1+\nu)\beta^2+1+\nu\right]\omega^2\overline{W}_n(s) \\ -s^2\overline{U}_n(s)=0\ , \tag{2.36}$$

and

$$\omega^2\left[-(1+\nu)n(n+1)+\beta^2(1-n(n+1)-\nu)n(n+1)\right]\overline{U}_n(s) \\ -\omega^2\beta^2 n(n+1)\left[1-n(n+1)-\nu\right]\overline{W}_n(s) \\ +2(1+\nu)\omega^2\overline{W}_n(s)+s^2\overline{W}_n=-\tilde{c}\left(as\overline{\Phi}_n(R=1,s)+\frac{A_n}{s}\right)\ . \tag{2.37}$$

2.7 Solution of Dimensionless Modal Problem and Finding $F_n(s)$

The Laplace-transformed problem for the n^{th} mode has three unknowns: $U_n(s)$, $W_n(s)$ and $F_n(s)$ (which is bundled into $\overline{\Phi}_n(R,s)$ for convenience). These three quantities are determined via the remaining three equations: the two shell equations in (2.36) and (2.37) and the acceleration boundary condition in equation (2.14). The key quantity of interest here is $F_n(s)$ which is the Laplace transform of the time-dependent modal amplitude that determines the entire dynamics of the fluid. The solution presented for this model along with the shell equations differ from all current spherical models (Hasheminejad et al., 2011).

2.7.1 Determining $F_n(s)$

Beginning with the acceleration boundary condition at $R = 1$, the Laplace-transformed solution must satisfy

$$\overline{\Phi}_R(\theta, R = 1, s) = -bs\overline{W}(\theta, s) \ , \tag{2.38}$$

and the modal form of this condition from equations (2.30) and (2.31) is

$$\overline{\Phi}_{nR}(R = 1, s) = -bs\overline{W}_n(s) \ . \tag{2.39}$$

Substituting $\overline{\Phi}_{nR}(R = 1, s)$ from equation (2.28) yields

$$F_n(s)\frac{\partial}{\partial R}\left(\sqrt{\frac{\pi}{2Rs}}I_{n+1/2}(Rs)\right)\Big|_{R=1} = -bs\overline{W}_n(s) \ . \tag{2.40}$$

It remains to determine $\overline{W}_n(s)$ from the shell equations (2.36) and (2.37). These are a system of two linear equations for $\overline{U}_n(s)$ and $\overline{W}_n(s)$ and it is convenient, before determining $\overline{W}_n(s)$, to make the definitions

$$\begin{aligned}
\gamma_1 &= (1+\beta^2)\omega^2[1-\nu-n(n+1)] \\
\gamma_2 &= \omega^2[(n(n+1)-1+\nu)\beta^2+1+\nu] \\
\gamma_3 &= \omega^2[-(1+\nu)n(n+1)+\beta^2(1-n(n+1)-\nu)n(n+1)] \\
\gamma_4 &= -\omega^2[-(1+\nu)n(n+1)+\beta^2(1-n(n+1)-\nu)n(n+1)]+2(1+\nu)\omega^2 \ .
\end{aligned} \tag{2.41}$$

With these definitions the shell equations (2.36) and (2.37) simplify to the form

$$\begin{aligned}(\gamma_1 - s^2)\overline{U}_n + \gamma_2\overline{W}_n &= 0 \\ \gamma_3\overline{U}_n + (\gamma_4 + s^2)\overline{W}_n &= -\left[a\tilde{c}s\overline{\Phi}_n + \tilde{c}A_n/s\right] \ ,\end{aligned} \tag{2.42}$$

and immediately

$$\overline{W}_n(s) = \frac{-(\gamma_1 - s^2)\left(a\tilde{c}s\overline{\Phi}_n(R=1,s) + \tilde{c}A_n/s\right)}{(\gamma_1 - s^2)(\gamma_4 + s^2) - \gamma_2\gamma_3} \ . \tag{2.43}$$

Then, from (2.40), $F_n(s)$ is obtained as

$$F_n(s) = \frac{bs(\gamma_1 - s^2)(a\tilde{c}s\overline{\Phi}_n(R=1,s) + \tilde{c}A_n/s)}{D} \ , \tag{2.44}$$

where the denominator term is

$$D = \frac{\partial}{\partial R}\left(\sqrt{\frac{\pi}{2Rs}}I_{n+1/2}(Rs)\right)\Big|_{R=1}\left((\gamma_1 - s^2)(\gamma_4 + s^2) - \gamma_2\gamma_3\right) \ . \tag{2.45}$$

A standard definition for the modified spherical Bessel function of the first kind is

$$i_n(z) = \sqrt{\frac{\pi}{2z}}I_{n+1/2}(z) \ . \tag{2.46}$$

Applying the chain rule in (2.45) and denoting $di_n/dz\Big|_{z=s} = i_n'(s)$,

$$D = si_n'(s)\left((\gamma_1 - s^2)(\gamma_4 + s^2) - \gamma_2\gamma_3\right) \ . \tag{2.47}$$

Rewriting the numerator in equation (2.44) slightly

$$F_n(s) = \frac{ab\tilde{c}s^2(\gamma_1 - s^2)\overline{\Phi}_n(R=1,s) + b\tilde{c}A_n(\gamma_1 - s^2)}{D} \ . \tag{2.48}$$

Cross-multiplying in equation (2.48) and combining $\overline{\Phi}(1,s)_n$ from equation (2.28) with the definition from equation (2.46) yields

$$F_n(s)D = ab\tilde{c}s^2(\gamma_1 - s^2)F_n(s)i_n(s) + b\tilde{c}A_n(\gamma_1 - s^2) \ . \tag{2.49}$$

Collecting terms in $F_n(s)$ and solving for $F_n(s)$ yields

$$F_n(s) = \frac{b\tilde{c}A_n(\gamma_1 - s^2)}{D - ab\tilde{c}s^2(\gamma_1 - s^2)i_n(s)} \ , \tag{2.50}$$

and substituting for D from equation (2.47), we arrive at

$$F_n(s) = \frac{b\tilde{c}A_n(\gamma_1 - s^2)}{si_n'(s) - ab\tilde{c}s^2(\gamma_1 - s^2)i_n(s)} \ . \tag{2.51}$$

The parameter, $ab\tilde{c}$, that controls the dynamics has emerged in the solution and this parameter is renamed

$$\alpha = ab\tilde{c} \ , \tag{2.52}$$

and then

$$F_n(s) = \frac{b\tilde{c}A_n(\gamma_1 - s^2)}{si_n'(s) - \alpha s^2(\gamma_1 - s^2)i_n(s)} \ . \tag{2.53}$$

To clarify notations for the remainder of the discussion, it is useful to write equations (2.28) and (2.29) using the compact form in equation (2.46) and then

$$\overline{\Phi}_n(R, s) = F_n(s)i_n(Rs) \ , \tag{2.54}$$

giving

$$\overline{\Phi}(R, \theta, s) = \sum_{n=0}^{\infty} F_n(s)i_n(Rs)P_n(\theta) \ . \tag{2.55}$$

The next step is to invert the n^{th} modal term $F_n(s)i_n(Rs)$.

2.7.2 Finding Modal Inverse by Inverting $F_n(s)i_n(Rs)$

The inverse is evaluated using the residue theorem in two steps: (i) the roots of the denominator of $F_n(s)$ are found and (ii) the ratio of the numerator of $F_n(s)$ multiplied by $i_n(Rs)$ and the derivative of the denominator is evaluated at these roots.

2.7.3 Roots

The roots of the denominator satisfy

$$i_n'(s)[(\gamma_1 - s^2)(\gamma_4 + s^2) - \gamma_2\gamma_3] - \alpha s(\gamma_1 - s^2)i_n(s) = 0 \ , \tag{2.56}$$

where a factor of s has been removed and the root at $s = 0$ yields a shift that is subtracted from the solution and does affect the dynamics. Substituting the recurrence formula

$$i_n'(s) = \frac{ni_{n-1} + (n+1)i_{n+1}}{2n+1} \tag{2.57}$$

into equation (2.56) and simplifying, we obtain

$$[ni_{n-1} + (n+1)i_{n+1}]\left[(\gamma_1 - s^2)(\gamma_4 + s^2) - \gamma_2\gamma_3\right] - \alpha s(2n+1)(\gamma_1 - s^2)i_n(s) = 0 \ . \tag{2.58}$$

The zeroes are confined to the imaginary axis since there is no exponential decay and $i_n(s)$ grows exponentially with real component and is oscillatory on the imaginary axis. In what follows, we use the fact that

$$i_n(i\mathcal{P}) = i^n j_n(\mathcal{P}) \ , \tag{2.59}$$

where $\mathcal{P}$ is real, $j_n(\mathcal{P})$ is related to the ordinary Bessel function of the first kind as

$$j_n(\mathcal{P}) = \sqrt{\frac{\pi}{2\mathcal{P}}} J_{n+1/2}(\mathcal{P}) \tag{2.60}$$

that oscillates with dying amplitude for $\mathcal{P}$ real.

If $s = i\mathcal{P}$ are the roots of equation (2.58) then

$$\begin{aligned}[nj_{n-1}(\mathcal{P}) - (n+1)j_{n+1}(\mathcal{P})]\left[(\gamma_1 + \mathcal{P}^2)(\gamma_4 - \mathcal{P}^2) - \gamma_2\gamma_3\right] + \\ \alpha\mathcal{P}(2n+1)(\gamma_1 + \mathcal{P}^2)j_n(\mathcal{P}) = 0 \ .\end{aligned} \tag{2.61}$$

2.7.4 Residues

The residue requires finding the derivative of the denominator of (2.53) and evaluating it at the roots of (2.56). It is shown in Appendix B that

$$(si_n'(s))' = \frac{1}{s}\left((s^2 + n^2)i_n - si_{n+1}\right) \ . \tag{2.62}$$

Differentiating the denominator of (2.53) with respect to s yields

$$\begin{aligned}(si_n'(s))'[(\gamma_1 - s^2)(\gamma_4 + s^2) - \gamma_2\gamma_3] \\ +si_n'(s)[-2s(\gamma_1 - \gamma_4) - 4s^3] - \alpha(2s\gamma_1 - 4s^3)i_n(s) \\ -\alpha s^2(\gamma_1 - s^2)i_n'(s) \ .\end{aligned} \tag{2.63}$$

Substituting for $(si_n'(s))'$ from equation (2.62) and applying the recurrence relation in equation (2.57), we arrive at

$$\begin{aligned}\frac{1}{s}[(s^2 + n^2)i_n - si_{n+1}][(\gamma_1 - s^2)(\gamma_4 + s^2) - \gamma_2\gamma_3] - 2\alpha s[\gamma_1 - 2s^2]i_n \\ s^2\left[\frac{ni_{n-1} + (n+1)i_{n+1}}{2n+1}\right]\left[2(\gamma_1 - \gamma_4) - 4s^2 - \alpha(\gamma_1 - s^2)\right] \ .\end{aligned} \tag{2.64}$$

To simplify the presentation, the numerator and denominator of $F_n(s)i_n(Rs)$ will be treated separately. The factor of $1/s$ in equation (2.63) is removed by multiplying top and bottom by s so that the numerator of $F_n(s)i_n(Rs)$ from equation (2.53) is

$$b\tilde{c}A_n s(\gamma_1 - s^2)i_n(Rs) \ , \tag{2.65}$$

and its denominator is

$$\begin{aligned}[(s^2+n^2)i_n - si_{n+1}][(\gamma_1 - s^2)(\gamma_4 + s^2) - \gamma_2\gamma_3] - 2\alpha s^2[\gamma_1 - 2\alpha s^2]i_n \\ + s^3\frac{ni_{n-1} + (n+1)i_{n+1}}{2n+1}[2(\gamma_1 - \gamma_4) - 4s^2 - \alpha(\gamma_1 - s^2)] \ .\end{aligned} \tag{2.66}$$

Recalling that $s = i\mathcal{P}$ and substituting from equation (2.59) the numerator may be rewritten as

$$b\tilde{c}A_n\mathcal{P}(\gamma_1 + \mathcal{P}^2)j_n(R\mathcal{P})i^n e^{i\mathcal{P}t} \ , \tag{2.67}$$

while the denominator is

$$\begin{aligned}[(n^2-\mathcal{P}^2)i^n j_n - i\mathcal{P}i^{n+1}j_{n+1}] \quad [\quad & (\gamma_1 + \mathcal{P}^2)(\gamma_4 - \mathcal{P}^2) - \gamma_2\gamma_3] + 2\alpha\mathcal{P}^2[\gamma_1 + 2\alpha\mathcal{P}^2]i^n j_n \\ + \quad & i^3\mathcal{P}^3\frac{ni^{n-1}j_{n-1} + (n+1)i^{n+1}j_{n+1}}{2n+1} \\ (\quad & 2(\gamma_1 - \gamma_4) + 4\mathcal{P}^2 - \alpha(\gamma_1 + \mathcal{P}^2)) \ .\end{aligned} \tag{2.68}$$

Dividing by i^n in the numerator and denominator in equations (2.67) and (2.68) respectively gives the numerator as

$$b\tilde{c}A_n\,(i\mathcal{P})\,(\gamma_1 + \mathcal{P}^2)j_n(R\mathcal{P})e^{i\mathcal{P}t} \ , \tag{2.69}$$

while the denominator is

$$\begin{aligned}[(n^2-\mathcal{P}^2)j_n + \mathcal{P}j_{n+1}][(\gamma_1 + \mathcal{P}^2)(\gamma_4 - \mathcal{P}^2) - \gamma_2\gamma_3] + 2\alpha\mathcal{P}^2[\gamma_1 + 2\alpha\mathcal{P}^2]j_n \\ - \mathcal{P}^3\frac{nj_{n-1} - (n+1)j_{n+1}}{2n+1}[2(\gamma_1 - \gamma_4) + 4\mathcal{P}^2 - \alpha(\gamma_1 + \mathcal{P}^2)] \ .\end{aligned} \tag{2.70}$$

At the complex conjugate root, $s = -i\mathcal{P}$, equation (2.69) becomes equal to its complex conjugate due to the $-i\mathcal{P}e^{-i\mathcal{P}\tau}$, while equation (2.70) is unchanged. Before summing the results for $s = \pm i\mathcal{P}$ it is convenient to note that there are a set of roots $m = 1, 2, 3, \cdots$ in equation (2.61) for each choice of $n = 0, 2, 3, \cdots$. Therefore the roots at $s = \pm i\mathcal{P}$ are relabelled as $s_{nm} = \pm i\mathcal{P}_{nm}$.

Adding both results for $s_{nm} = \pm i\mathcal{P}_{nm}$ in equations (2.69) and (2.70) leads to the numerator as

$$\mathcal{N}_{nm}(R)\left[-2\sin(\mathcal{P}_{nm}\tau)\right] = b\tilde{c}A_n\mathcal{P}_{nm}(\gamma_1 + \mathcal{P}_{nm}^2)j_n(R\mathcal{P}_{nm})\left[-2\sin(\mathcal{P}_{nm}\tau)\right] \ , \quad (2.71)$$

and this form is also intended to define $\mathcal{N}_{nm}(R)$. The denominator remains the same for $s_{nm} = \pm i\mathcal{P}_{nm}$ and

$$\begin{aligned}\mathcal{D}_{nm} &= [(n^2 - \mathcal{P}_{nm}^2)j_n + \mathcal{P}_{nm}j_{n+1}][(\gamma_1 + \mathcal{P}_{nm}^2)(\gamma_4 - \mathcal{P}_{nm}^2) - \gamma_2\gamma_3] \\ &+ 2\alpha\mathcal{P}_{nm}^2[\gamma_1 + 2\alpha\mathcal{P}_{nm}^2]j_n \\ &- \mathcal{P}_{nm}^3\frac{nj_{n-1} - (n+1)j_{n+1}}{2n+1}[2(\gamma_1 - \gamma_4) + 4\mathcal{P}_{nm}^2 - \alpha(\gamma_1 + \mathcal{P}_{nm}^2)] \ . \quad (2.72)\end{aligned}$$

Referring to equation (2.55) the inverse of $\overline{\Phi}(R, \theta, s)$ follows from equations (2.71) and (2.72) as

$$\Phi(R, \theta, \tau) = \sum_{n=0}^{\infty}\sum_{m=1}^{m=\infty}\frac{\mathcal{N}_{nm}(R)}{\mathcal{D}_{nm}}P_n(\theta)\left[-2\sin(\mathcal{P}_{nm}\tau)\right] \ . \quad (2.73)$$

2.8 Results

The total pressure or impact $\underset{\sim}{P}_0(\tau)$ from equation (2.18) is

$$\underset{\sim}{P}_0(\tau) = f(\theta)e^{-\tau/\tilde{\beta}} \ , \quad (2.74)$$

where $\exp(-\tau/\tilde{\beta})$ in equation (2.74) is assumed to be unity given that $\tau \ll \tilde{\beta} = 150$. The θ dependence

$$f(\theta) = \sum_{n=0}^{\infty}A_nP_n(\cos(\theta)) \quad (2.75)$$

is represented as a series of A_n terms. If a step input is applied over $0 \leq \theta \leq \theta^*$ then

$$\begin{aligned}A_0 &= \frac{1 - \cos(\theta^*)}{2} \\ A_n &= \frac{P_{n-1}(\cos(\theta^*)) - P_{n+1}(\cos(\theta^*))}{2} \quad (2.76)\end{aligned}$$

The Legendre-Fourier series coefficients $\mathcal{N}_{nm}(R)/\mathcal{D}_{nm}$ are found subject to the constraint to minimize the squared error between the exact solution and its Legendre-Fourier representation. Thus, the least-squares pathway that optimally approximates

the solution in a least-squares sense simply follows the decreasing magnitude of the coefficients $\mathcal{N}_{nm}(R)/\mathcal{D}_{nm}$ in equation (2.73).

In this way, the double summation in (2.73) is reduced to a single sum that depends upon the radius R. The least-squares pathway through the pair of indices n and m is followed down to a minimum magnitude and a formal summation index used here is $\mathcal{L}(R) = 1, 2, 3, \cdots, N(R)$ where the maximum numbered coefficient is $N(R)$, and then

$$\Phi(R,\theta,\tau) = \sum_{\mathcal{L}=1}^{\mathcal{L}=N(R)} \frac{\mathcal{N}_{n(\mathcal{L})m(\mathcal{L})}(R)}{\mathcal{D}_{n(\mathcal{L})m(\mathcal{L})}} P_{n(\mathcal{L})}(\theta) \left[-2\sin(\mathcal{P}_{n(\mathcal{L})m(\mathcal{L})}\tau)\right] \ . \tag{2.77}$$

2.8.1 Space-Time Evolution

The solution $\Phi(R,\theta,\tau)$ in equation (2.77) is evaluated using MATLAB. The results presented in Figures 2.3-2.6 are computed after organizing the magnitudes into descending order and retaining sufficient terms to obtain a desired level of accuracy. Early times show the development of a leading pressure wave, and by $t = 0.8$ a distinct wave can be seen. This 'wave' can be tracked and observed travelling through the sphere through all times, in particular near the outer radii of the sphere. Near the center of the sphere, this 'wave' starts to breaks down as it meets other rebounding waves as can be seen at $t = 1.6$. This can also be explained by the lack of organized coherence of the energies near the center of the sphere seen later on in Figure 2.17. Continuing to proceed through time, the wave can be seen to reach the back surface of the sphere at $t = 2.0$. This feature represents the contrecoup feature of head impacts. Onwards from $t = 2.2$ to $t = 4.8$ the first internal pressure wave continues travelling through the sphere and encounters other waves rebounding from the surface of the sphere causing local minimums and maximums which can be seen for instance at $t = 3.8$.

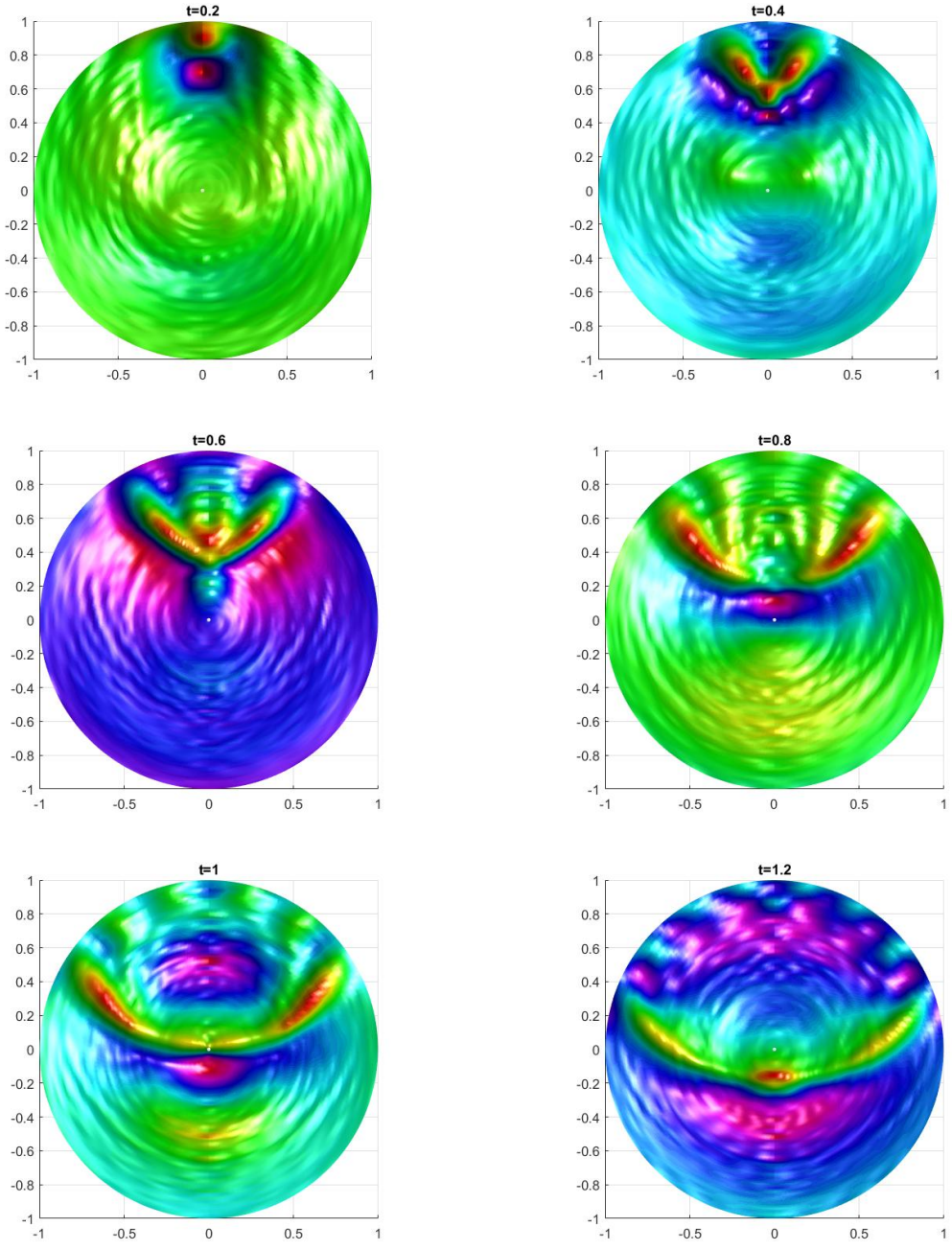

Figure 2.3: Solution from $t = 0.2$ to $t = 1.2$.

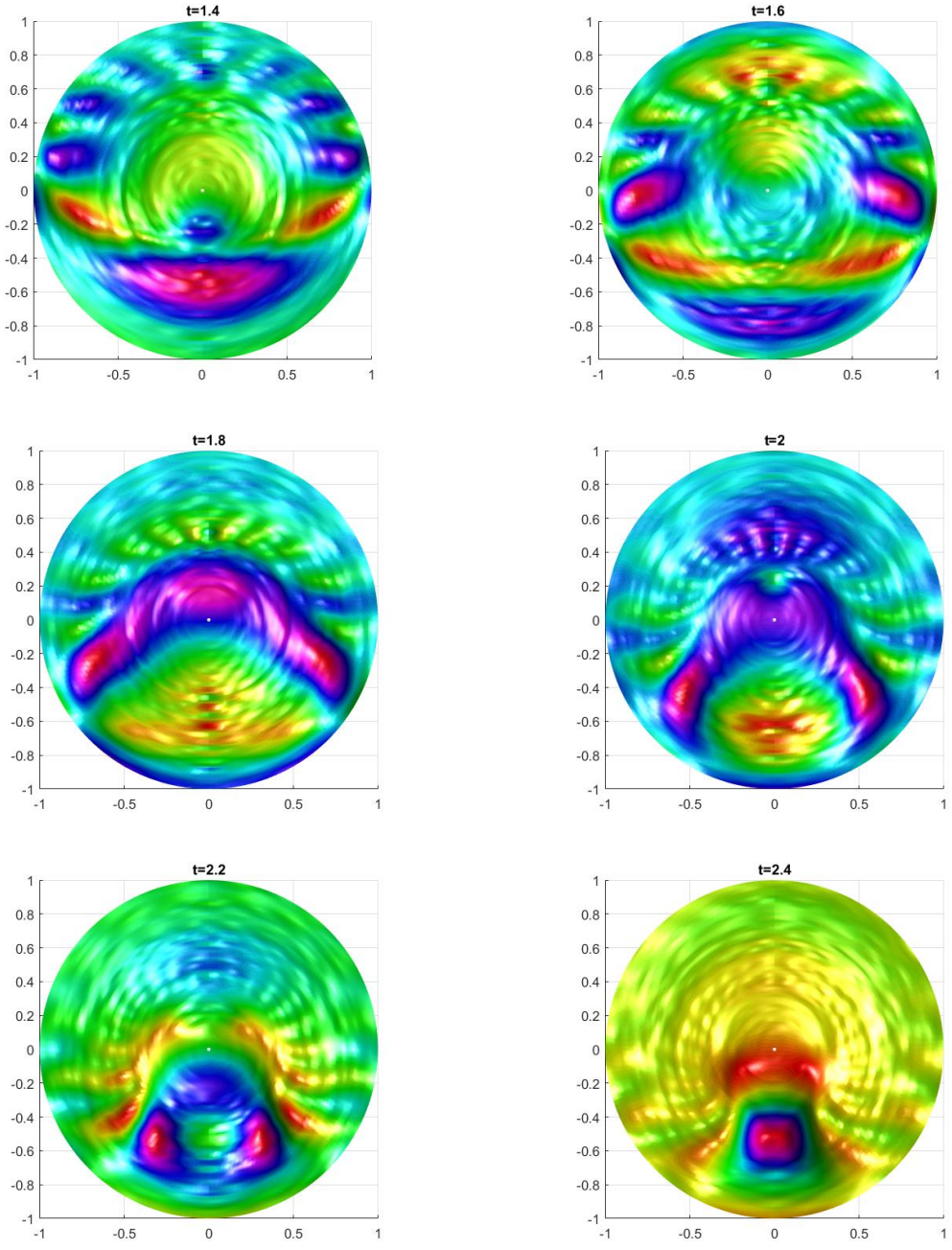

Figure 2.4: Solution from $t = 1.4$ to $t = 2.4$.

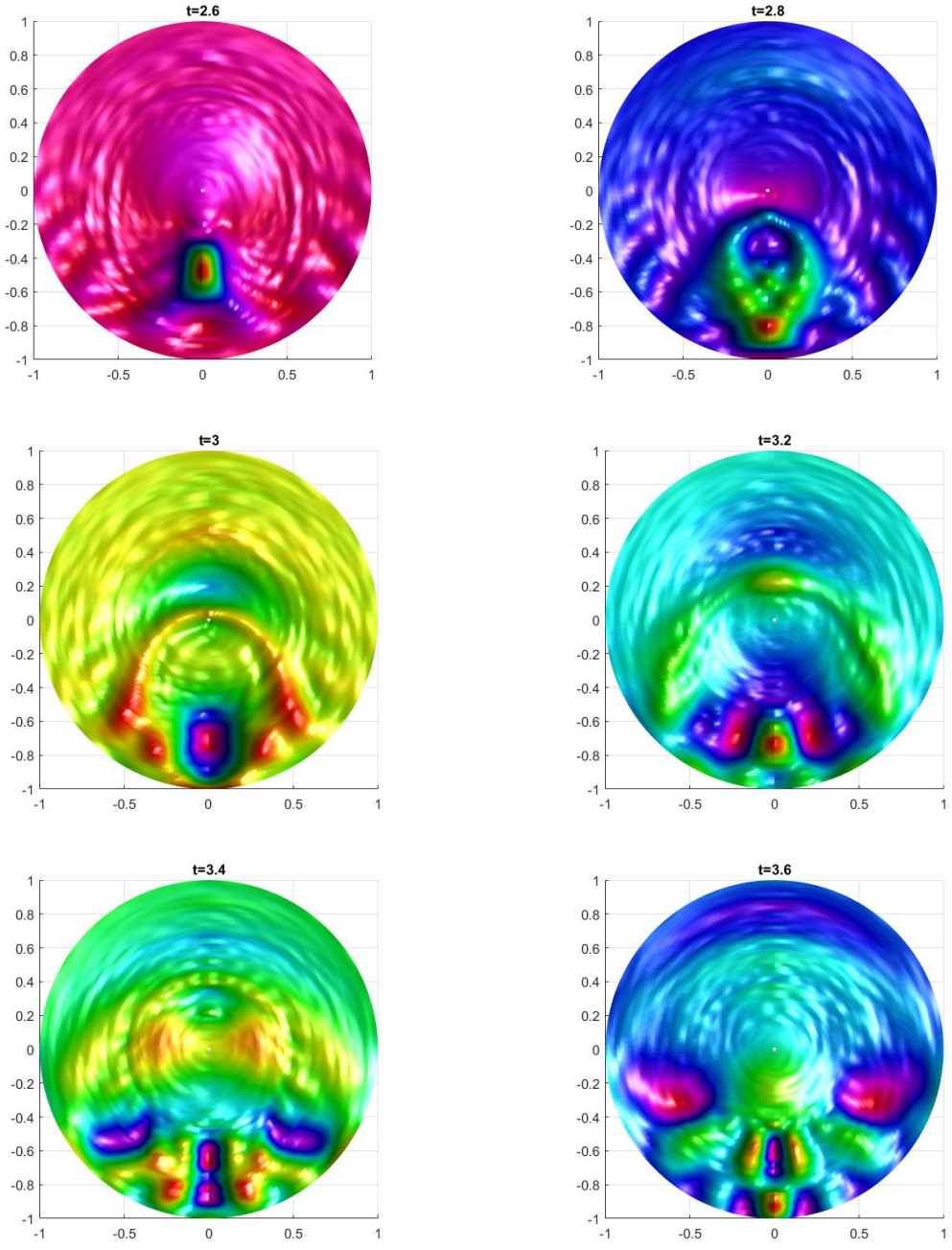

Figure 2.5: Solution from $t = 2.6$ to $t = 3.6$.

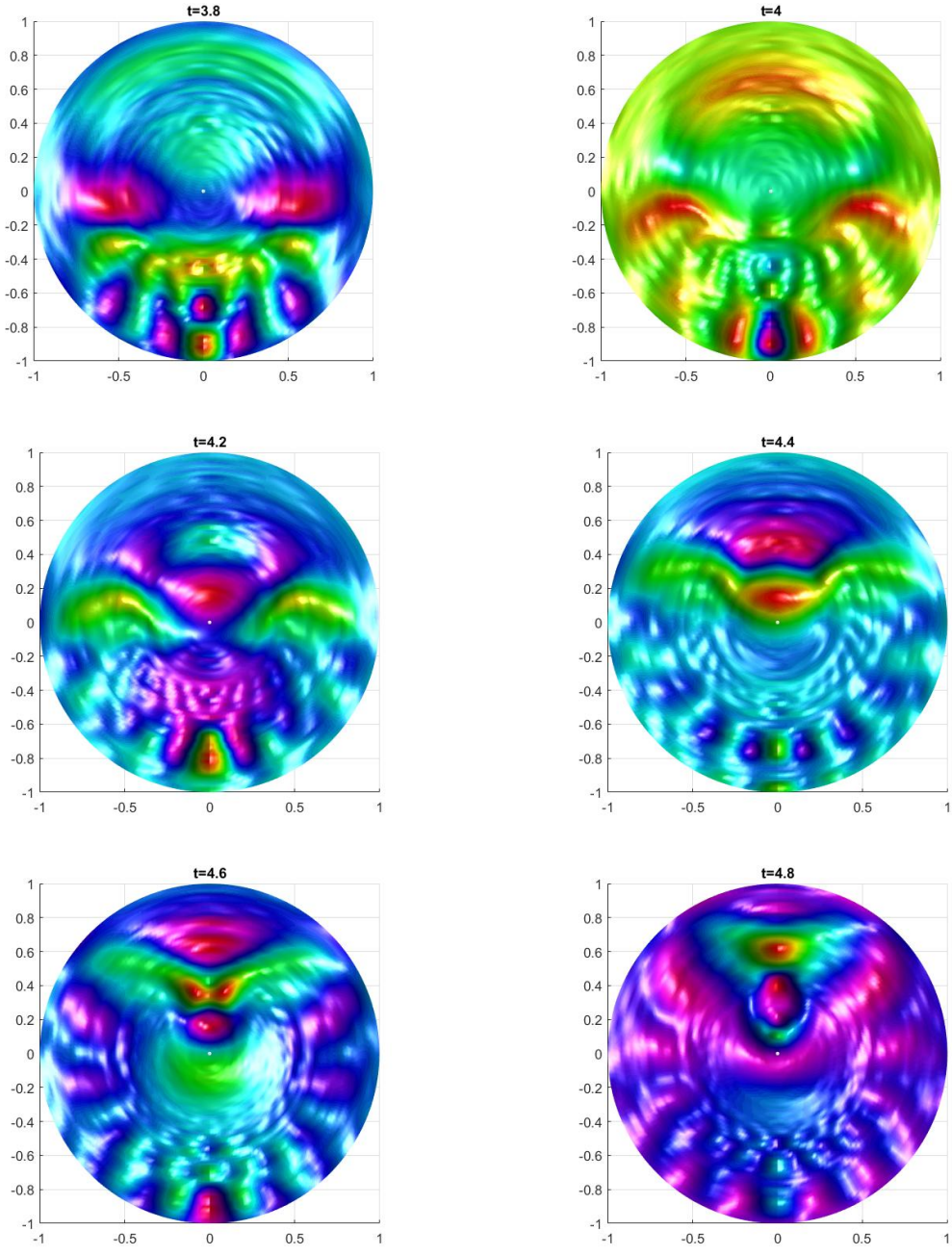

Figure 2.6: Solution from $t = 3.8$ to $t = 4.8$.

An approximation for the results was also computed and can be seen in Figures 2.7-2.10. This was accomplished by keeping only residues and amplitudes that represented 80% of the total energy used in the previous figures. By observation, the same features described in the previous solution can also be seen in the approximate solution. This

means that the key features of the dynamics are bound upon and rely heavily on only a few amplitudes and frequencies as discussed in a later section. It can therefore be concluded that 80% of the overall energy was sufficient in describing the dynamics of the solution.

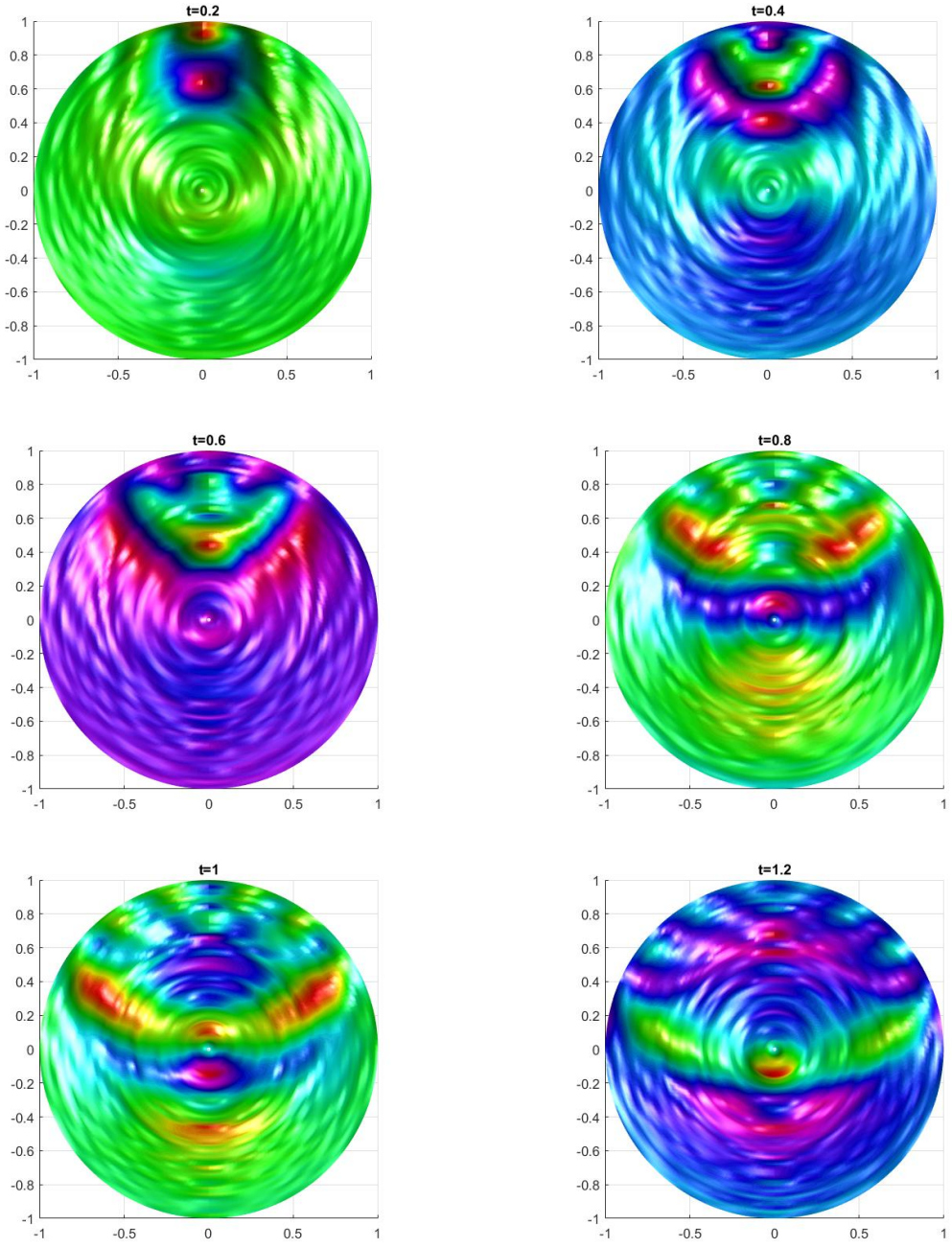

Figure 2.7: Approximate solution from $t = 0.2$ to $t = 1.2$.

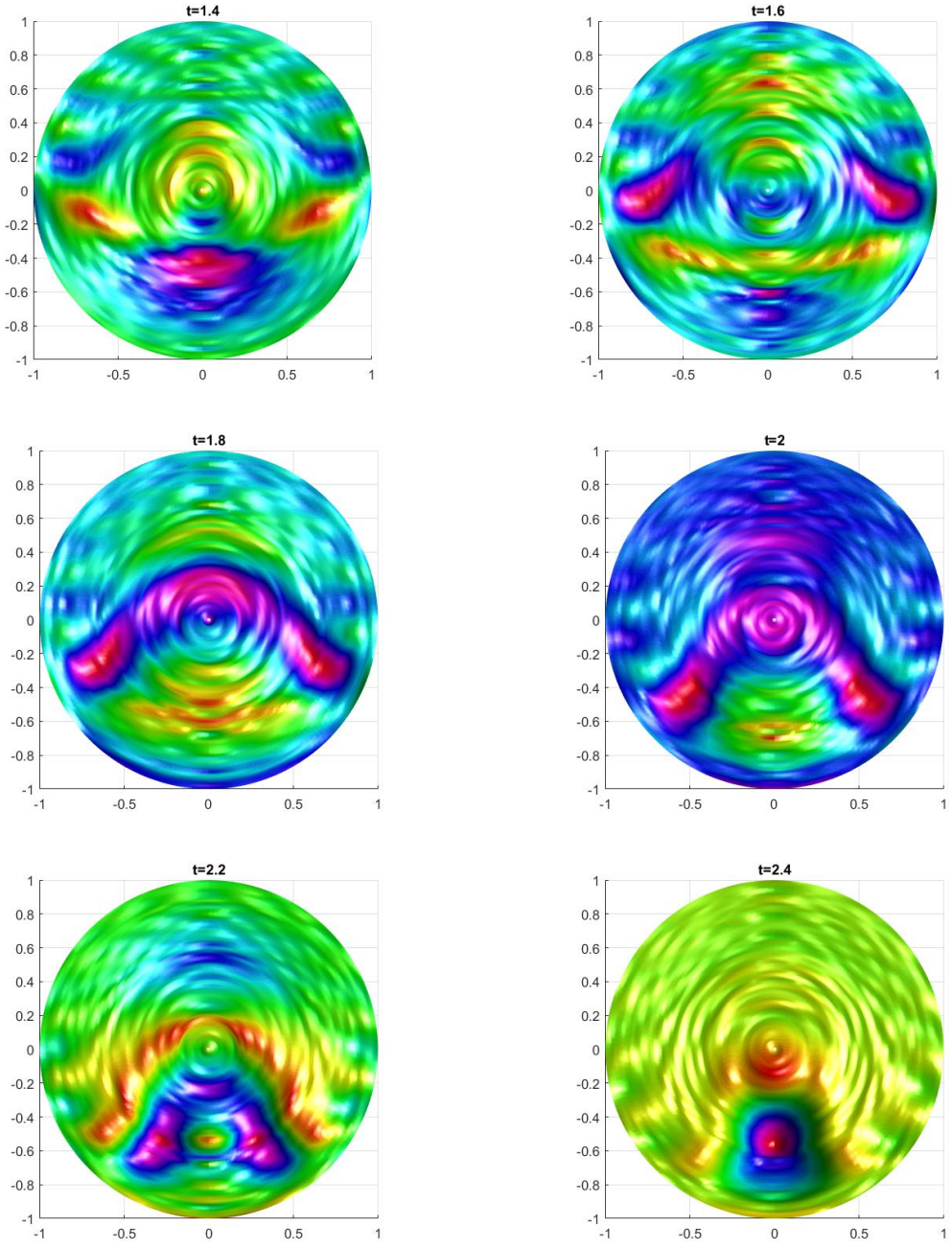

Figure 2.8: Approximate solution from $t = 1.4$ to $t = 2.4$.

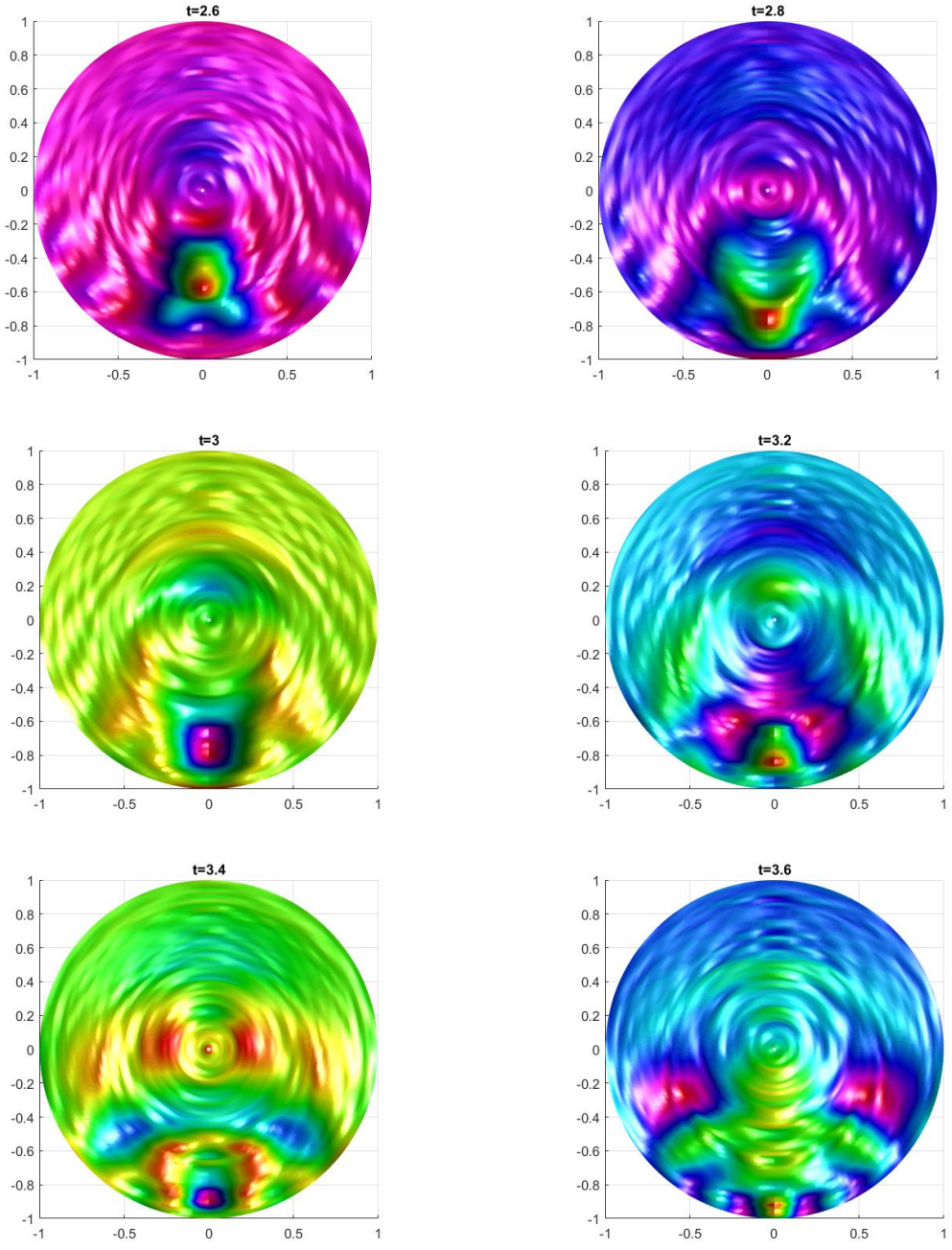

Figure 2.9: Approximate solution from $t = 2.6$ to $t = 3.6$.

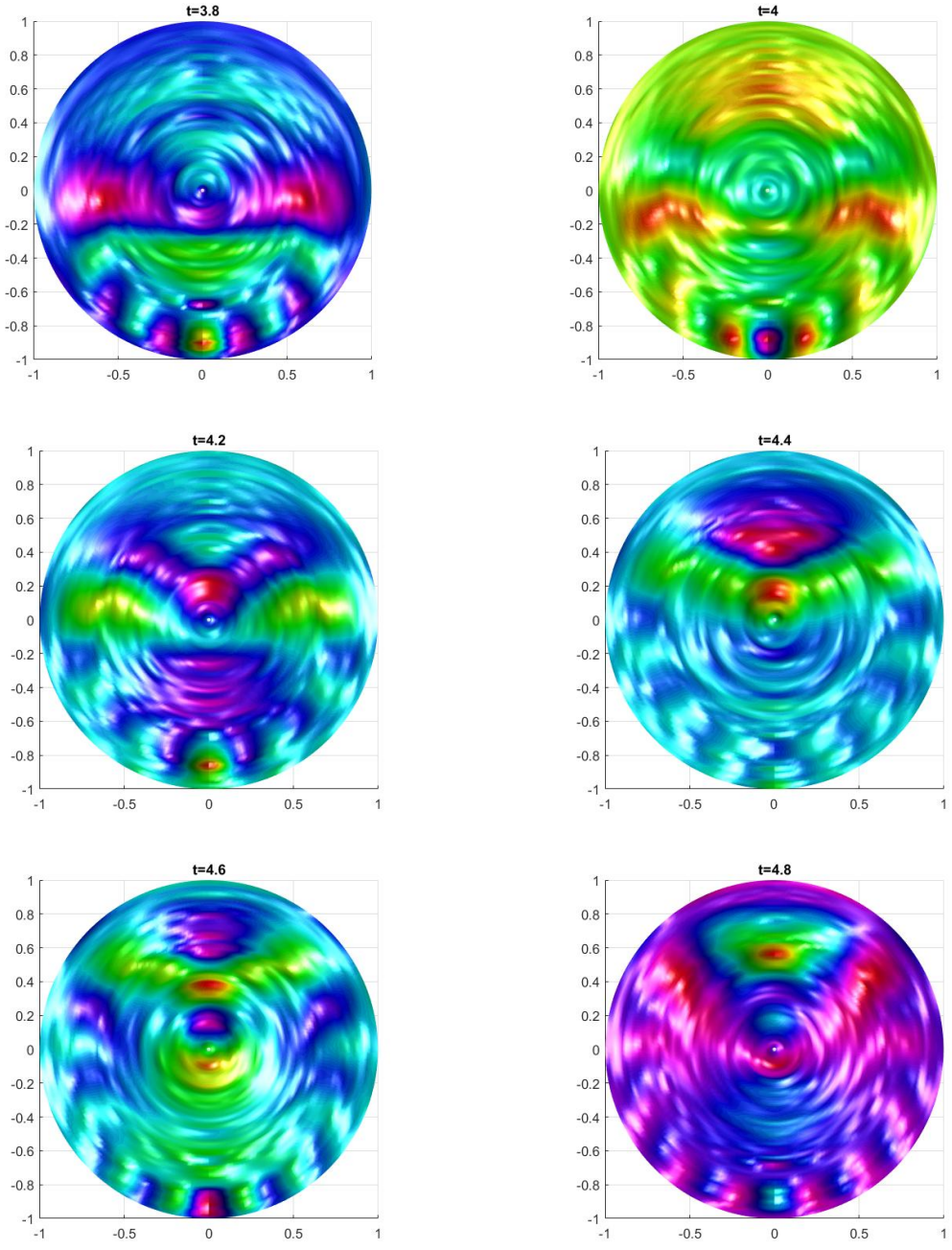

Figure 2.10: Approximate solution from $t = 3.8$ to $t = 4.8$.

To better understand the clinical implications of the solutions, we can compare the solution to the brain scan seen in Figure 2.11.

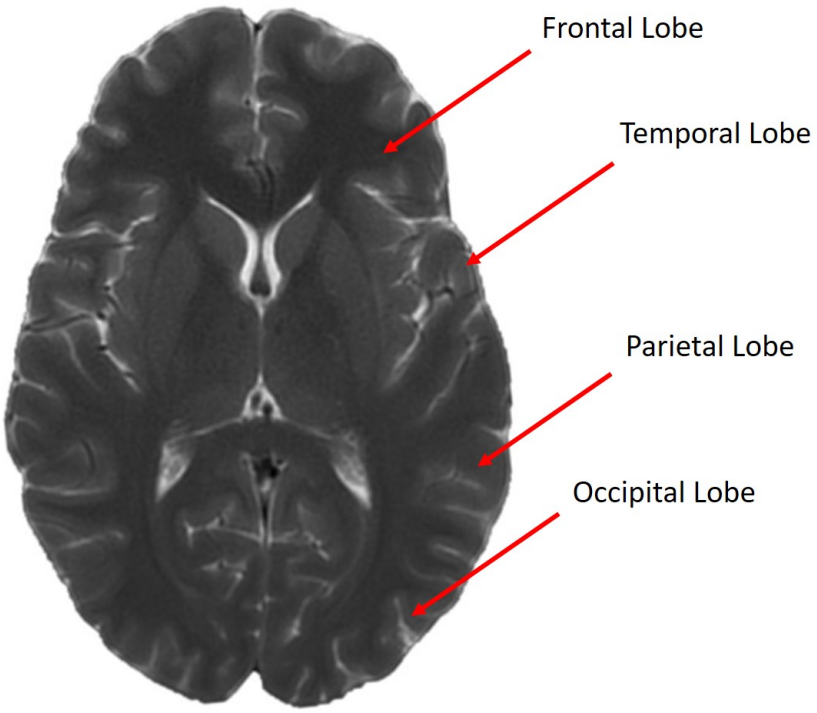

Figure 2.11: MRI scan of a brain (Courtesy of Darvesh, S., Maritime Brain Tissue Bank, 2016)

This image is used as an overlay for the obtained solutions to determine visually the anatomical structures of the brain that are affected by the pressure waves in the solution, in Figures 2.12-2.15.

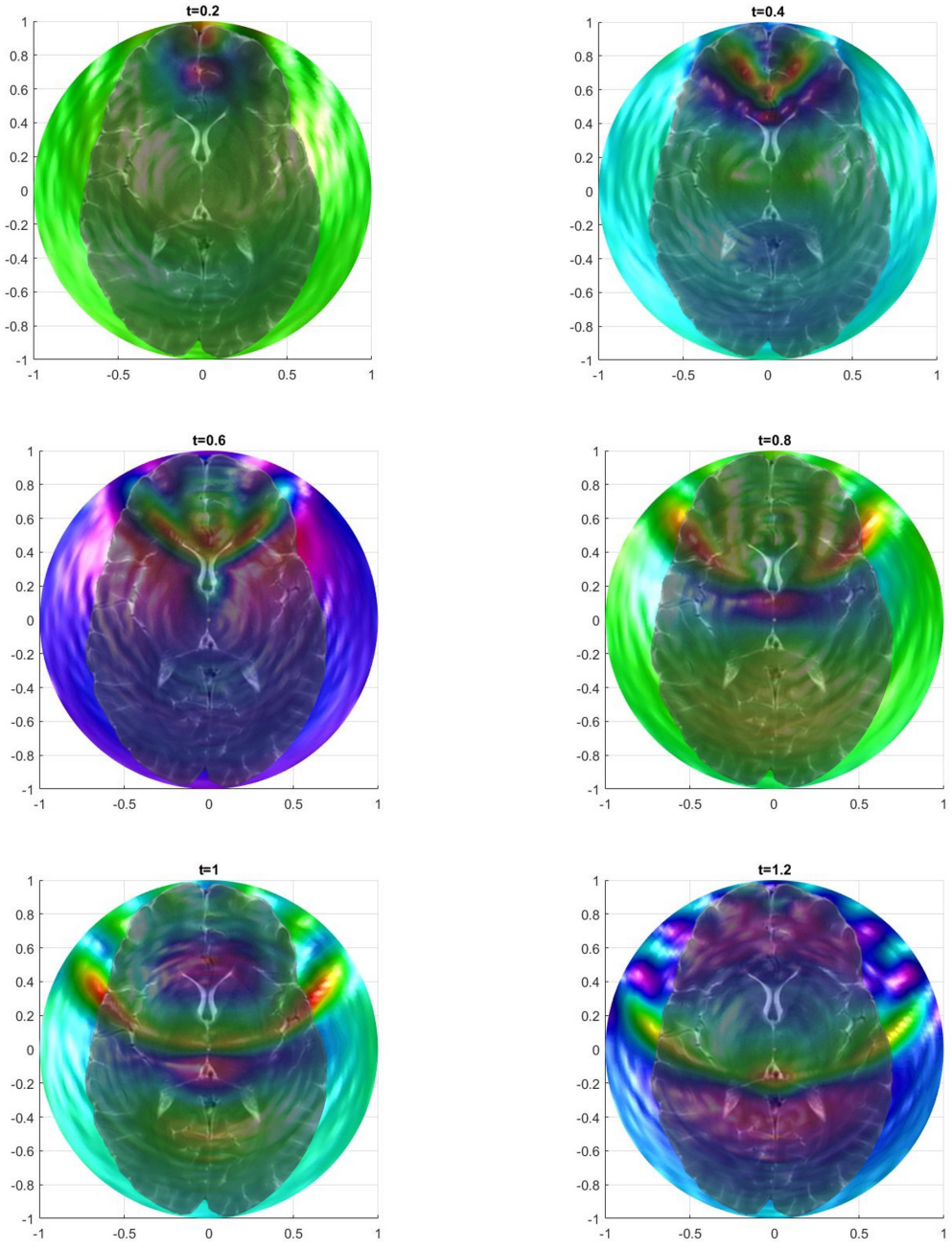

Figure 2.12: Solution with brain overlay from $t = 0.2$ to $t = 1.2$.

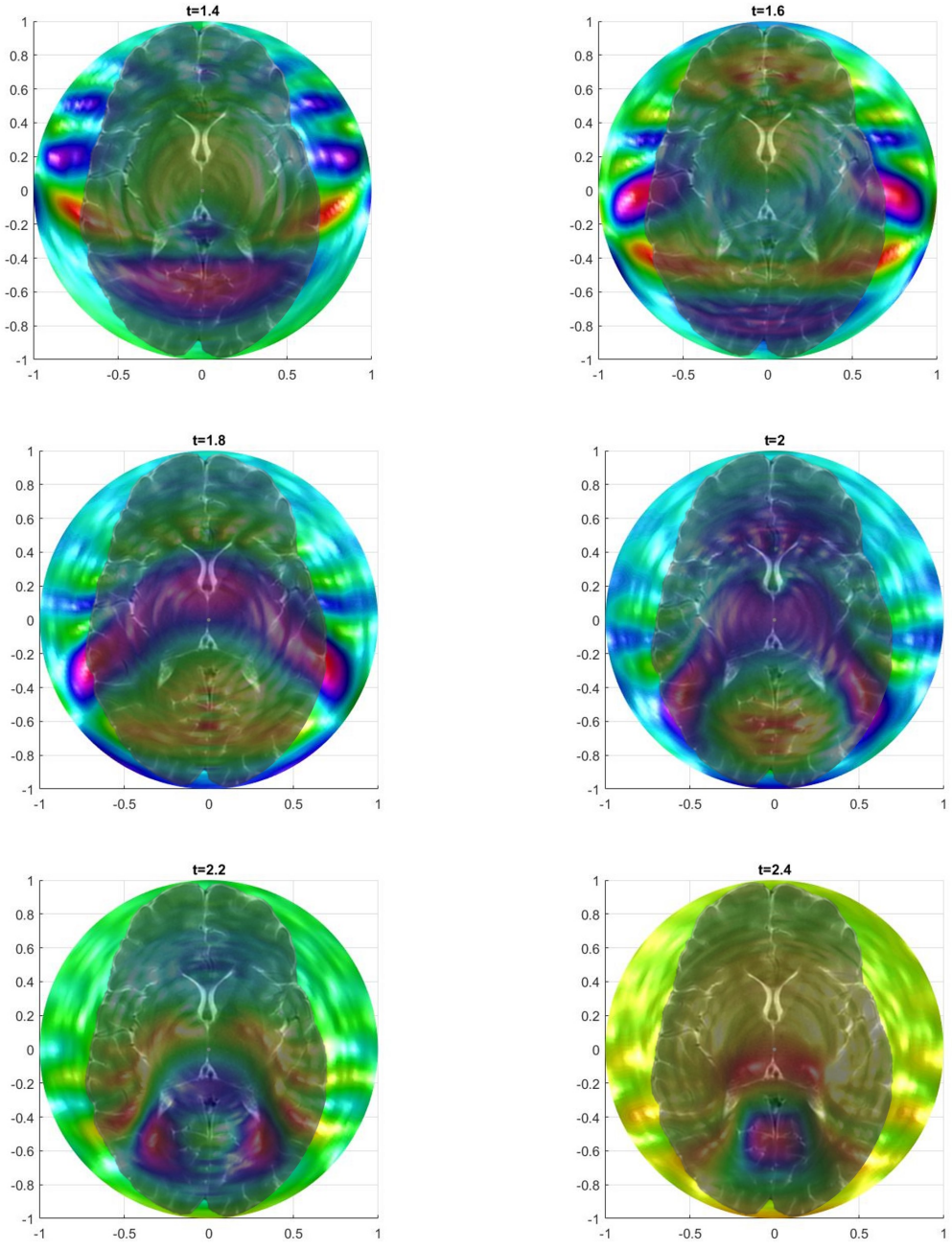

Figure 2.13: Solution with brain overlay from $t = 1.4$ to $t = 2.4$.

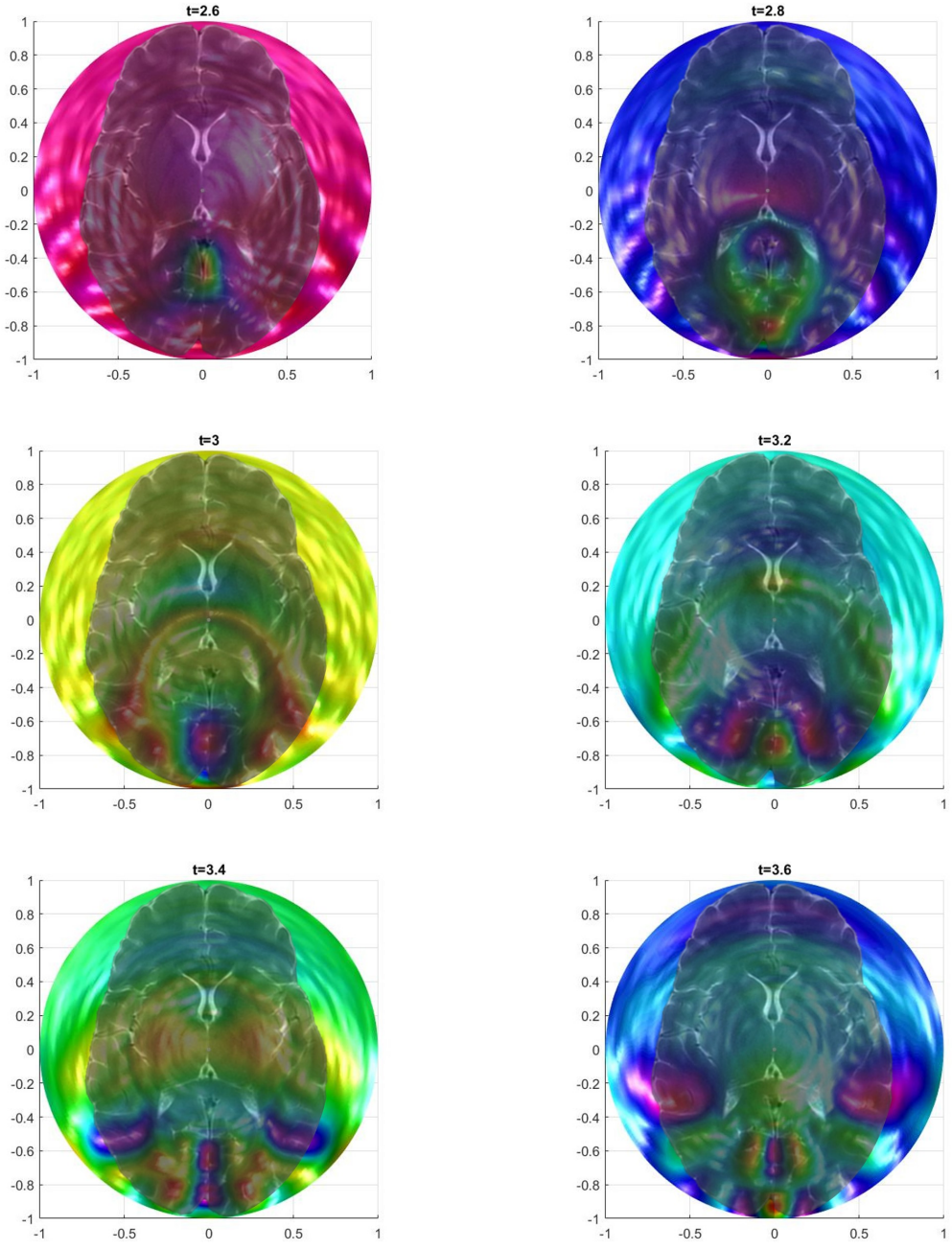

Figure 2.14: Solution with brain overlay from $t = 2.6$ to $t = 3.6$.

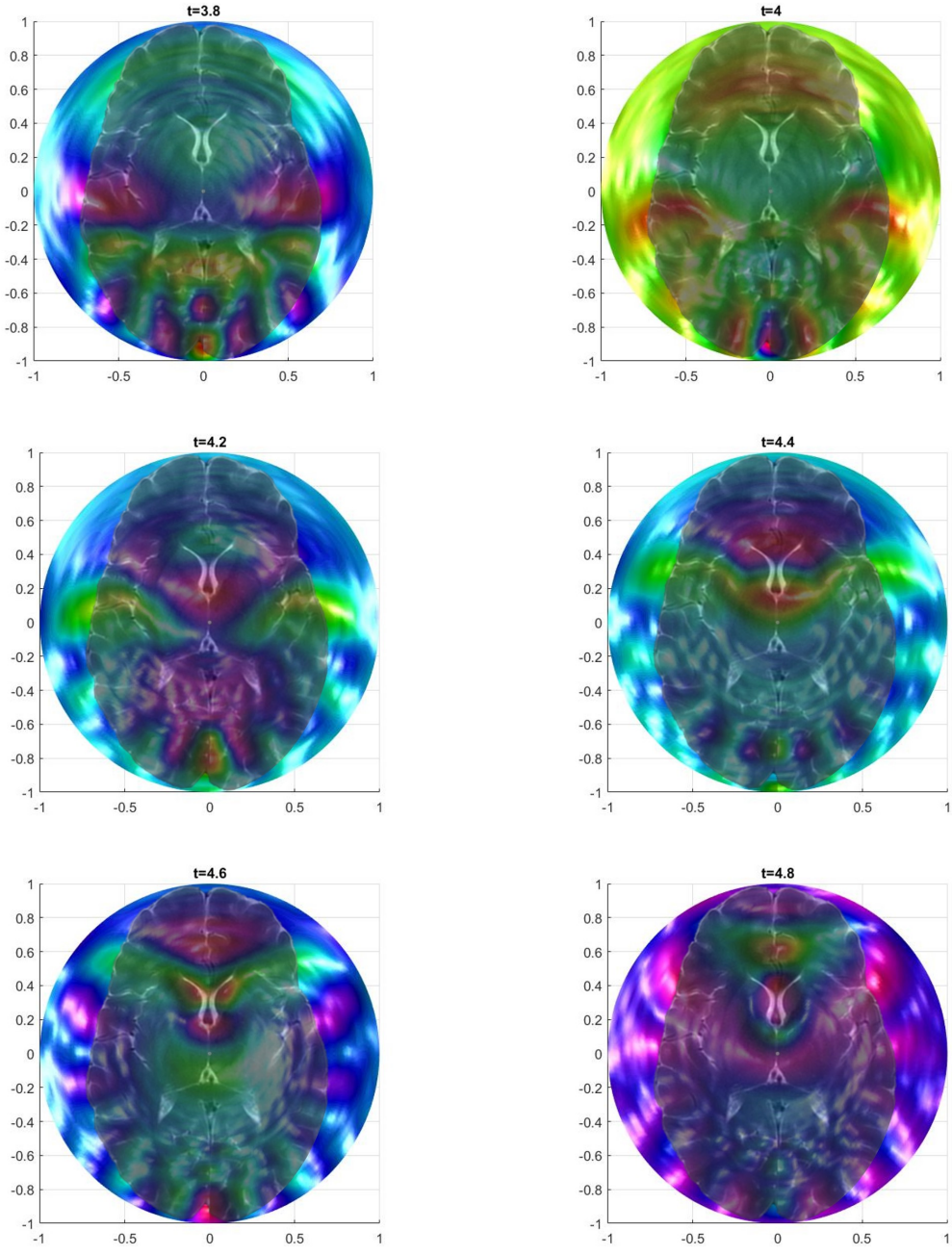

Figure 2.15: Solution with brain overlay $t = 3.8$ to $t = 4.8$.

By combining the brain image and the series solution, a clear pattern emerges of what structures within the brain are affected. The coup feature of the impact which can be seen at $t = 0.2$ and again at $t = 4.8$ is predominantly confined to within the frontal lobe of the brain. Similarly, the contrecoup feature, seen at $t = 2.0$, can be seen primarily affecting the occipital lobe and the cerebellum. Throughout all times, the pressure waves can be seen travelling around the outer regions of the brain, involving all the brain regions from the frontal to temporal lobes and the parietal to occipital lobes. Near the center of the brain coherence is lost and many pressure waves exist simultaneously. Here in the center, these waves focus on the limbic system of the brain, including the hippocampus, among other structures part of the temporal lobe. These affected structures can also be seen to reflect the symptoms and effects seen during traumatic brain injuries and concussions. For example, memory loss is commonly seen with these types of injuries which can be linked to the temporal lobe and specifically the hippocampus. As well, problems with attention and concentration are other common symptoms of traumatic brain injuries which can be linked to the frontal lobe. The structures that can be seen affected in the above figures are in agreement with clinical understanding and the symptoms and effects of traumatic brain injuries can be linked back to these affected structures (Barkhoudarian et al., 2011; Blennow et al., 2012; Signoretty et al., 2011)

2.8.2 Energy Transfer – Numerical vs Analytical

The work presented so far is a standard approach to solving a straightforward linear equation. A significant effort was required to construct the analytical solution and using this form to construct the figures presented in the previous section could have been done also via a numerical solution. Note also that the rescaling analysis and discovery of a single dimensionless group governing the dynamics was done without recourse to the analytical solution. While there may be issues surrounding analytical versus numerical solution accuracy, it is a reasonable assertion that the analytical solution has not provided any additional insight into the problem that could not have been found via a numerical solution. So it follows that one would ask, 'Why bother obtaining the analytical solution at all?' To answer this question, it is useful to focus on the coup-contrecoup feature which is generally of greatest practical interest. This

feature is striking in the application considered here mainly because of the level of simplicity of its evolution. This simplicity stands in direct contrast to the degree of complexity of the analytical solution. The key qualitative feature of the coup-contrecoup feature is its high degree of coherence which implies that there must be an underlying simplicity in the way energy is transferred within the sphere. Previous studies have presented analyses of the free vibrations of a fluid-filled shell, as summarized by Engin and Liu (1970) and Huang (1969), and formed the basis for the model considered here. Those results of free vibration are essentially extended here into the fluid and it is found that the fluid-filled shell may be viewed as a collection of shells that transfer energy in a very simple way that retains wave coherence until the center of the shell is reached. Therefore, in this section the solution $\Phi(R, \theta, \tau)$ in equation (2.77) is re-examined and a qualitative energy transfer function is found. This function shows how energy is transferred as the pressure-wave makes its way around the sphere in space-time. As a result, the precise way that the linear model represents energy transfer between various radii as a function of spatial and temporal frequencies is made clear. Stated another way, the energy description reduces the sphere to a set of concentric shells where the movement of energy through these shells follows some very simple rules and this provides insight into the high degree of coherence seen in the coup-contrecoup evolution. In other words, such an energy transfer function remains outside of the scope of any numerical solution and this fact alone provides a justification for constructing the analytical solution.

2.8.3 Qualitative Energy Transfer Function

In this section the relationship between frequency in time via $\sin(\mathcal{P}_{n(\mathcal{L})m(\mathcal{L})}\tau)$ and frequency in space through $P_{n(\mathcal{L})}(\theta)$ and the dependence of these two quantities upon R is considered. It is found that the least-squares approach presents a simple relationship between frequency in space and time that varies continuously with the radius R and essentially determines the movement of energy through frequency in space-time. The energy in a wave is proportional to its squared amplitude which in this problem is $(\mathcal{N}_{nm}(R)/\mathcal{D}_{nm})^2$. Therefore, the amplitudes, for each value of the dimensionless radius R, are respectively re-arranged into descending order to run between a maximum of unity and a minimum of zero. The energy contributed by each amplitude,

used to construct the 'exact' solution presented in the previous section, is depicted in Figure 2.16 where the scaled energy is shown as a function of the radius, spatial frequency, and temporal frequency.

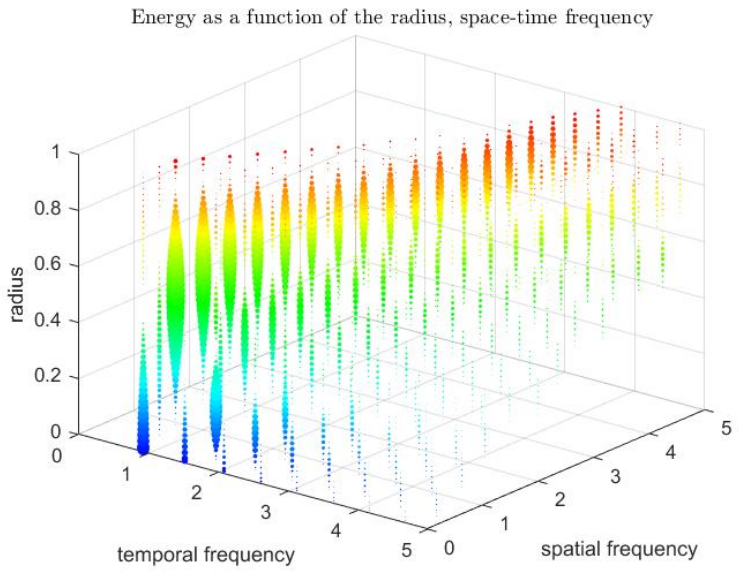

Figure 2.16: Energy as a function of the radius, spatial frequency, and temporal frequency.

In this plot, the radius is shown as the color of the dots as well as on the vertical axis, where dark blue represents $R = 0$, the center of the sphere, and red represents $R = 1$, the outer radius of the sphere. As well, a fourth dimension is added into the plot; the diameter of the dots represents the amplitudes. Larger dots are associated with larger amplitudes and therefore larger energies. The spatial frequency associated with the *mode* n is qualitatively approximated as $n/4$ where n is the *order* of the Legendre polynomial. The sense of spatial periodicity used here is a convenient variable and is defined such that, for example, $\mathcal{P}_4(x)$ is symmetric on $-1 \leq x \leq 1$ and qualitatively has period 1 over $0 \leq x \leq 1$. It will become apparent below that choosing $n/4$ also leads to an approximately unit dimensionless wave speed for the outer and moderate radii of the sphere. The temporal frequency is related to the *root* in the complex root associated with the Legendre order and is $\mathcal{P}_{n(\mathcal{L})m(\mathcal{L})}/(2\pi)$.

To get a better understanding of the key features of this plot, a 2D projection has been provided in Figure 2.17.

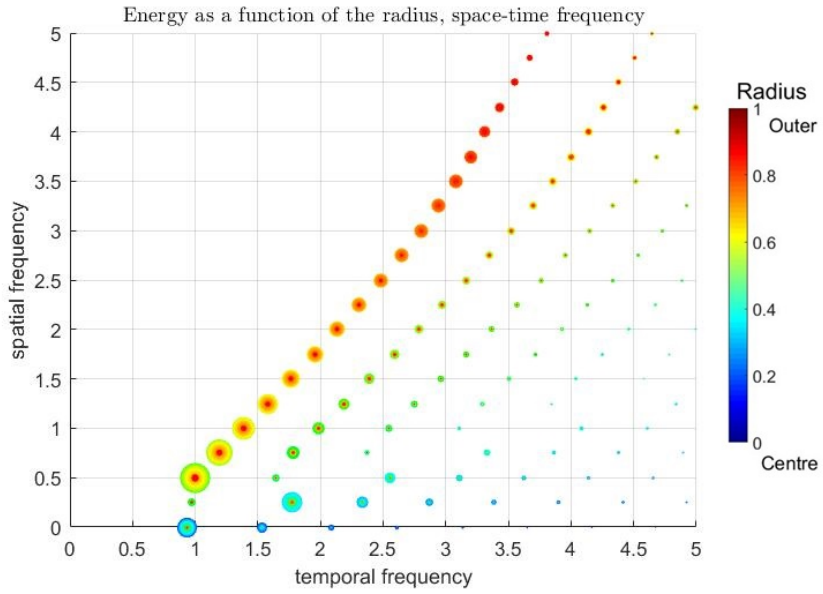

Figure 2.17: 2D projection of energy levels.

It is clear from Figure 2.17, that energy near the outer portions of the sphere (coloured red) is spread over a range of spatial-temporal frequencies that are approximately linearly related. This linear relationship observed for radii near the shell strongly resembles the same relationship seen in free vibrations of the shell and implies that the shell dynamics are transferred into the interior region to some extent. It can also be seen that for moderate values (green) of the dimensionless radius, the spatial-temporal relationship occupies primarily two lines and the relationship between spatial and temporal frequencies is slightly more complex. Continuing into the center of the sphere (blue), all of the energy is now heavily concentrated into a range of space-temporal frequencies that occupy many lines and thus any relationship between spatial and temporal frequencies is lost. Finally, the slope of the lines seen above approximate unity and thus the wavespeed in the outer (red) and moderate radii (green) approximates unity (via $n/4$ definition of the spatial frequency above) and this leads to coherence of the coup-contrecoup feature. The same is not true however nearer the center (blue) where a single relation between the spatial-temporal frequencies cannot be found and many wavespeeds exist.

Referring to the amplitudes (diameter of the dots) in Figures 2.16 and 2.17, the main feature of interest is that the maximum amplitudes appear at moderate radii

(green) at lower spatial-temporal frequencies. This concentration of energy represents the coherence of the coup-contrecoup feature that is itself primarily located at moderate radii which can be seen for example at $t = 2.0$ in Figure 2.4. Continuing into the center of the sphere (blue) the amplitudes are maximal near the origin of the spatial-temporal frequencies and show no clear relationship as the amplitudes decrease in size. This latter observation is consistent with what is seen in the previous section where the wave 'breaks up' when it nears the center of the sphere and becomes less coherent as compared with what is seen at outer and moderate radii.

The comparison of the 'exact' and approximate series earlier showed that 80% of the energy was sufficient to describe much of the qualitative dynamics. Therefore, Figures 2.16 and 2.17 are reconsidered in Figure 2.18 and its projection in Figure 2.19 for only amplitudes representing 80% of the total energy.

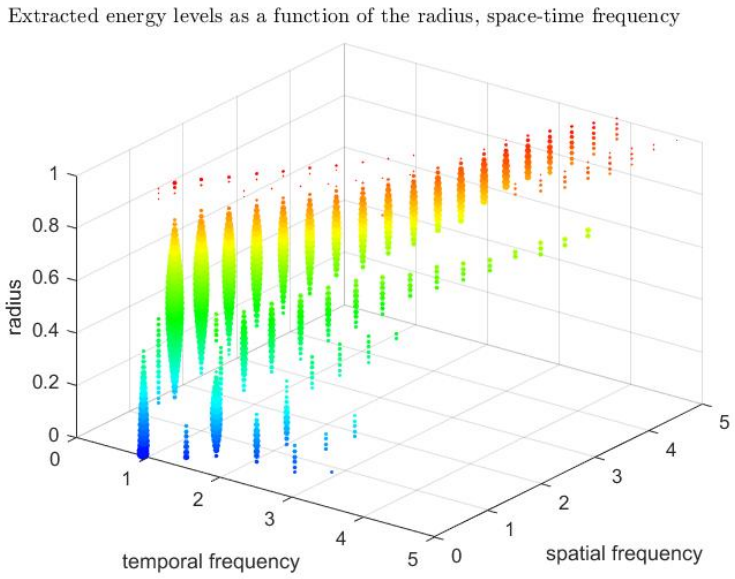

Figure 2.18: Extracted energy levels representing 80% of the total energy

When considering 80% of the overall energy it is apparent that near the outer region of the sphere (red) the energy is captured by roughly a dozen amplitudes confined to a single spatial-temporal frequency line. Moving further inward (green) the same energy is confined to two lines, as in the 'exact' results, and again there is no relation nearer the center of the sphere (blue). The most important overall observation is that most (80%) of the total energy is bound up in few (approximately

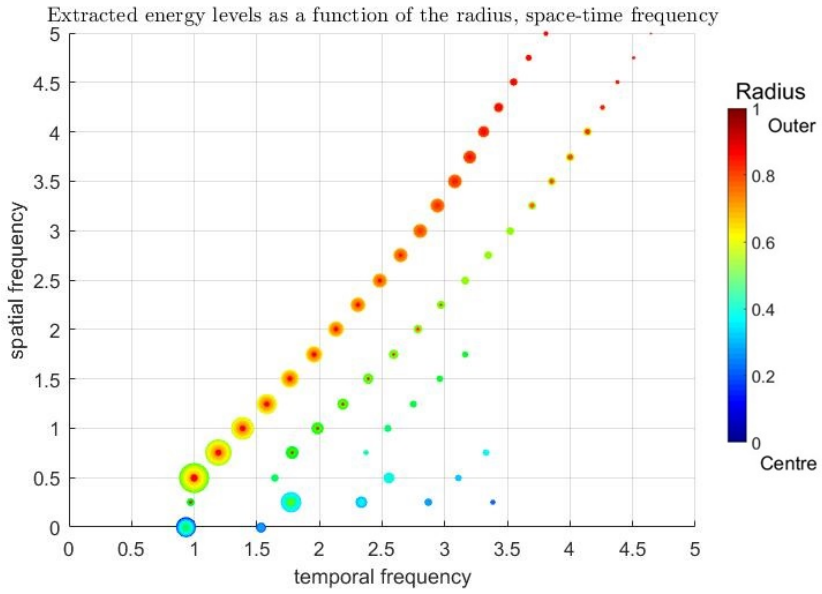

Figure 2.19: Projection of extracted energy levels representing 80% of the total energy

a dozen) amplitudes where these show a nearly linear relationship between space and temporal frequencies for moderate radii. This slope of the linear relation between the spatial and temporal frequencies approximates unity in the outer 60% of the sphere and this leads to the coherence observed for moderate radii in the space-time series given above. Nearer the center of the shell the energy coherence is lost and energy is spread in a complex fashion through space-time frequencies. These observations provide a basis for understanding how energy is moved through different radii within the fluid and the shell may be viewed as a set of concentric shells that simply transfer energy along lines in the spatial-temporal frequency plane. This description closely mirrors that seen for free vibrations of the shell (Engin and Liu, 1970) and implies that the shell dynamics are preserved to some extent and penetrate the fluid. It is interesting that the coup-contrecoup seen for $t = 2.0$ is organized from waves that proceed into the center and re-emerge in a coherent fashion with the implication being that the simplicity of the dynamics continues even after the waves enter and exit the center of the sphere where there is relatively little coherence.

Chapter 3

Conclusion

We have considered a mathematical model of percussive pressure events impacting a spherical, fluid-filled shell with circular symmetry. The fluid is assumed to be irrotational and its velocity is described by a linear potential that is coupled to the shell. An analytic solution to this model was obtained and used to simulate interactions between the skull structure (shell) and brain tissue (fluid) during a percussive impact.

It was found that the response of the linear model is dependent upon a single dimensionless group that represents the relationship between the shell and fluid properties, $a \cdot b \cdot \tilde{c}$. For the application of the model to head injury this parameter is large compared with unity ($\mathcal{O}$ 10) since the skull is considerably more rigid than the brain tissue. The main objective of the thesis was to find a simplified description of the coup-contrecoup feature of the response to a percussive step-impact. This clear occurrence of the coup-contrecoup feature implies a coherence in space-time that may be extracted from the solution of the coupled potential and shell response equations. In particular, the Legendre-Fourier series is a least squares approach to the solution and thus the solution amplitudes are directly related to the energy content of each contributing wave in the separated series solution. It was found to be useful to consider the energy as a function of the radius for a qualitative spatial frequency of the Legendre polynomials and the temporal frequencies of sinusoidal component. In particular, the primary contributors in space-time to the pressure wave have a nearly linear relationship in space-time frequency and this linearity is a direct measure of wave coherence. It was found that for radii exceeding approximately one-half of the sphere the linear relationship and coherence persist, while there is a sharp drop in coherence within the one-tenth of the sphere center. Thus, the energy perspective shows how the response of the fluid-filled sphere moves energy in a coherent fashion in the outer portion and less so in central regions. Given most waves are damped, it is likely that the coherence of the waves is the most important clinical aspect.

In practice, it is the accumulated effect of sub-concussive glancing blows that is difficult to diagnose and treat due to the nature of its progression. This problem was not considered here, but what is of greater interest is that the work presented here is useful to furthering our understanding of that problem. To date, progress on sub-concussive effects has been elusive and, as outlined in the introduction, both percussive and viscous (rotation) models consistently underpredicted its effects. The primary feature that delineates percussion and viscous effect is time scale: percussive effects are temporally fast, spatially small, while viscous effects are relatively slower temporally and spatially larger. Including both percussive and viscous effects into a single numerical model has not been done due to computational and memory overheads; the fast, percussive model greatly increases the requirements for accuracy in both space and time. Therefore it will be of great interest to include viscosity into the linear model in a simplistic way (Joseph, 2003). Finally, there are no studies in the literature surrounding the stochastic nature of concussion.

Hence, it is proposed that a model be constructed that considers all three aspects: percussion, viscosity (inertial effects), and stochasticity. The model is not intended to be 'more exacting' by inserting an increasing number of features, but will attempt to uncover generic features of the fast and slow coupling between percussion and viscous effects in the presence of stochasticity. A way forward, that will be considered in the future, is to view the percussive and viscous aspects as independent to first order. This assumption will allow for the solution of the viscous and percussive problems to be independently constructed. The key to this problem is that the coupling between the two effects involves the detection of windows of vulnerability in the brain tissue, due to the viscous component, that are made sensitive to percussive effects. Stated another way, the viscous effects induces local shearing of brain tissue that may expose small regions of tissue to additional injury from percussive effects. Monte Carlo simulation of the entire process will lead to the ability to analyze risk of injury. This approach where percussive and viscous effects work in concert to create greater injury may provide a mechanism to explain why neither approach has yet provided an adequate explanation.

Bibliography

Abramowitz, M. and Stegun, I. (1964). *Handbook of Mathematical Functions*. National Bureau of Standards.

Aubry, M., Cantu, R., Dvorak, J., Graf-Baumann, T., Johnston, K., Kelly, J., Levell, M., McCroy, P., Meeuwisse, W., and Schamasch, P. (2002). Summary and agreement statement of the first international conference on concussion in sport, vienna 2001. recommendations for the improvement of safety and health of athletes who may suffer concussive injuries. *British Journal of Sports Medicine*, 36:6–10.

Bar-Kochba, E., Guttag, M., Sett, S., Franck, J. A., McNamara, K., Crisco, J. J., Blume, J., and Franck, C. (2012). Finite element analysis of head impact in contact sports. In *SIMULIA Community Conference*.

Bar-Kochba, E., Scimone, M. T., Estrada, J. B., and Franck, C. (2016). Strain and rate-dependent neuronal injury in a 3d in vitro compression model of traumatic brain injury. *Scientific Reports*, 6.

Barkhoudarian, G., Hovda, D. A., and Giza, C. C. (2011). The molecular pathophysiology of concussive brain injury. *Clinics in Sports Medicine*, 30:33–48.

Blennow, K., Hardy, J., and Zetterberg, H. (2012). The neuopathology and neurobiology of traumatic brain injury. *Neuron*, 76:886–899.

Bolouri, H. and Zetterberg, H. (2015). *Brain Neurotrauma: Molecular, Neuropsychological, and Rehabilitation Aspects*, chapter Animal Models for Concussion: Molecular and Cognitive Assessments - Relevance to Sport and Military Concussions. CRC Press.

Bonds, G. B., Edwards, W. W., and Spradley, B. D. (2014). Advancements in concussion prevention, diagnosis, and treatment. *The Sport Journal*.

Bradshaw, D. and Morfey, C. (2001). Pressure and shear responses in brain injury models. Technical report, University of Southampton; First Technology.

Cantu, R. (1992). Cerebral concussion in sport. management and prevention. *Sports Medicine*, 14:64–74.

Chan, H. S. and Liu, Y. K. (1974). The asymmetric response of a fluid-filled spherical shell - a mathematical simulation of a glancing blow to the head. *Journal of Biomechanics*, 7:43–59.

Choe, M. C. (2016). The pathophysiology of concussion. *Current Pain and Headache Reports*, 20(42):1–10.

Cloots, R., van Dommelen, J., Kleiven, S., and Geers, M. (2010). Traumatic brain injury at multiple length scales: Relating diffuse axonal injury to discrete axonal impairment. Technical report, Eindhoven University of Technology; Royal Institure of Technology, Sweden.

Council, N. R. (2014). *Review of Department of Defense Test Protocols for Combat Helmets*. National Academy Press.

Duma, S., Manoogian, S., Bussone, W., Brolinson, P., Goforth, M., Donnenwerth, J., Greenwald, R., Chu, J., and Crisco, J. (2005). Analysis of real-time head accelerations in collegiate football players. *Clinical Journal of Sport Medicine*, 15:3–8.

Engin, A. E. (1969). The axisymmetic response of a fluid-filled spherical shell to a local radial impulse - a model for head injury. *Journal of Biomechanics*, 2:325–241.

Engin, A. E. and Liu, Y. K. (1970). Axisymmetic response of a fluid-filled spherical shell in free vibrations. *Journal of Biomechanics*, 3:11–22.

Flierl, M. A., Stahel, P. F., Beauchamp, K. M., Morgan, S. J., Smith, W. R., and Shohami, E. (2009). Mouse closed head injury model induced by a weight-drop device. *Nature Protocols*, 4:1328–1337.

Foda, M. A. A.-E. and Marmarou, A. (1994). A new model of diffuse brain injury in rats. part 2: Morphological characterization. *Journal of Neurosurgery*, 80:301–313.

Frost, C. (2011). *Anatomy of the Concussion: More Serious than Meets the Eye?* PhD thesis, University of South Florida.

Gavett, B. E., Cantu, R. C., Shenton, M., Lin, A. P., Nowinski, C. J., McKee, A. C., and Stern, R. A. (2011). Clinical appraisal of chronic traumatic encephalopathy: current perspectives and future directions. *Current Opinion in Neurology*, 24:525–531.

Goldsmith, W. (2001). The state of head injury biomechanics: Past, present, and future: Part 1. *Critical Reviews in Biomedical Engineering*, 29(5 & 6):441–600.

Goldsmith, W. and Monson, K. L. (2005). The state of head injury biomechanics: Past, present, and future part 2: Physical experimentation. *Critical Reviews in Biomedical Engineering*, 33(2):105–207.

Gupta, R. K. and Przekwas, A. (2013). Mathematical models of blast-induced tbi: current status, challenges, and prospects. *Frontiers in Neurology*, 4(59):1–21.

Guskiewicz, K., Marshall, S., Bailes, J., McCrea, M., Cantu, R., Randolph, C., and Jordan, B. (2005). Association between recurrent concussion and late-life cognitive impairment in retired professional football players. *Neurosurgery*, 57:719–726.

Guskiewicz, K. and Mihalik, J. (2011). Biomechanics of sport concussion: quest for the elesive injury threshold. *Exercise and Sport Sciences Reviews*, 39:4–11.

Hasheminejad, S. M., Bahari, A., and Abbasion, S. (2011). Mode model and simulation of acoustic pulse interaction with a fluid-filled hollow elastic sphere through numerical laplace inversion. *Applied Mathematical Modelling*, 35:22–49.

Huang, H. (1969). Transient interaction of plane acoustic waves with a spherical elastic shell. *The Journal of the Acoustical Society of America*, 45(3):661–670.

Joseph, D. (2003). Viscous potential flow. *Journal of Fluid Mechanics*, 479:191–197.

Junger, M. C. and Feit, D. (2003). *Sound, Structures and Their Interaction*. MIT Press Ltd.

Kabadi, S. V., Hilton, G. D., Stoica, B. A., Zapple, D. N., and Faden, A. I. (2010). Fluid-percussion induced traumatic brain injury model in rats. *Nature Protocols*, 5:1552–1563.

Marmarou, A., Foda, M. A. A.-E., van den Brink, W., Campbell, J., Kita, H., and Demetriadou, K. (1994). A new model of diffuse brain injury in rats. part 1: Pathophysiology and biomechanics. *Journal of Neurosurgery*, 80:291–300.

McKee, A. C., Cairns, N. J., Dickson, D. W., Folkerth, R. D., Keene, C. D., Litvan, I., Perl, D. P., Stein, T. D., Vonsattel, J.-P., Stewart, W., Tripodis, Y., Crary, J. F., Bieniek, K. F., Dams-OConnor, K., Alvarez, V. E., Gordon, W. A., and the TBI/CTE group (2016). The first ninds/nibib consensus meeting to define neuropathological criteria for the diagnosis of chronic traumatic encephalopathy. *Acta Neuropathologica*, 131:75–86.

McKee, A. C., Cantu, R. C., Nowinski, C. J., Hedly-Whyte, E. T., Gavett, B. E., Budson, A. E., Santini, V. E., Lee, H.-S., Kubilus, C. A., and Stern, R. A. (2009). Chronic traumatic encephalophathy in athletes: Progressive tauopathy following repetitive head injury. *Journal of Neuropathology and Experimental Neurology*, 68:709–735.

Meaney, D. F. and Smith, D. H. (2011). Biomechanics of concussion. *Clinics in Sports Medicine*, 30:19–vii.

Miller, R. T., Marhulies, S. S., Leoni, M., Nonaka, M., Chen, X., Smith, D. H., and Meaney, D. F. (1998). Finite element modeling approaches for predicting injury in an experimental model of severe diffuse axonal injury. *Stapp Car Crash Journal*, 42:155–167.

Moore, D. F., Jrusalem, A., Nyein, M., Noels, L., Jaffee, M. S., and Radovitzky, R. A. (2009). Computational biology - modeling of primary blast effects on the central nervous system. *NeuroImage*, 47:T10–T20.

of Standards, N. I. and Technology (2016). Digital library of mathematical functions. http://dlmf.nist.gov/, Release 1.0.14 of 2016-12-21. F.W.J. Olver, A.B. Olde Daalhuis, D.W. Lozier, B.I. Schneider, R.F. Boisvert, C.W. Clark, B.R. Miller and B.V. Saunders, eds.

Omalu, B., DeKosky, S., Minster, R., Kamboh, M., Hamilton, R., and Wecht, C. (2005). Chronic traumatic encephalopathy in a national football league player. *Neurosurgery*, 57:128–134.

Ommaya, A. and Gennarelli, T. (1974). Cerebral concussion and traumatic unconsciousness: Correlation of experimental and clinical observations on blunt head injuries. *Brain*, 97:633–654.

Signoretty, S., Lazzarino, G., Tavazzi, B., and Vagnozzi, R. (2011). The pathophysiology of concussion. *Physical Medicine and Rehabilitation*, 3:359–368.

Smith, D., Meaney, D., and Shull, W. (2003). Diffuse axonal injury in head trauma. *Journal of Head Trauma Rehabilitation*, 18:307–316.

Stevenson, T. (2006). *Simulation of Vehicle-Pedestrian Interaction*. PhD thesis, University of Canterbury.

Takhounts, E., Eppinger, R., Campbell, J., Tannous, R., Power, E., and Shook, L. (2003). On the development of the simon finite element head model. *Stapp Car Crash Journal*, 47:107–133.

Thibault, L., Meaney, D., Anderson, B., and Marmarou, A. (1992). Biomechanical aspects of a fluid percussion model of brain injury. *Journal of Neurotrauma*, 9:311–322.

Thompson, H. J., Lifshitz, J., Marklund, N., Grady, M. S., Graham, D. I., Hovda, D. A., and McIntosh, T. K. (2005). Lateral fluid percussion brain injury: A 15-year review and evaluation. *Journal of Neurotrauma*, 22:42–75.

Viano, D. C., Casson, I. R., Pellman, E. J., Zhang, L., and King, A. I. (2005). Concussion in professional football: Brain responses by finite element analysis: Part 9. *Neurosurgery*, 57:891–916.

Wei, E. P., Kontos, H. A., Dietrich, W. D., Povlishock, J. T., and Ellis, E. F. (1981). Prostaglandins and free radicals in brain injury. *Circulation Research*, 48:95–103.

Zhang, J., Yoganandan, N., Pintar, F., and Gennarelli, T. (2006). Role of translational and rotational accelerations on brain strain in lateral head impacts. *Biomedical Sciences Instrumentation*, 42:501–506.

Zhang, L., Yang, K., and King, A. (2004). A proposed injury threshold for mild traumatic brain injury. *Journal of Biomechanical Engineering*, 126:226–236.

Appendix A

Separation of Dimensional Shell Equations

The dimensional form is separated here to allow for comparison with what is found in the literature and is easily moved into a dimensionless form immediately afterward.

The homogeneous form of the shell equations (2.3) and (2.4) are

$$\begin{aligned} u_{\theta\theta} + \cot(\theta)u_\theta - (\nu + \cot^2(\theta))u - \frac{\beta^2}{1+\beta^2}w_{\theta\theta\theta} \\ -\frac{\beta^2}{1+\beta^2}\cot(\theta)w_{\theta\theta} + \left[\frac{1+\nu}{1+\beta^2} + \frac{\beta^2}{1+\beta^2}\left(\nu + \cot^2(\theta)\right)\right]w_\theta \\ -\frac{a^2}{1+\beta^2}u_{tt} = 0 \ , \end{aligned} \tag{A.1}$$

and the radial shell displacements $w(\theta, t)$ satisfy

$$\begin{aligned} \beta^2 u_{\theta\theta\theta} + 2\beta^2\cot(\theta)u_{\theta\theta} - \left[(1+\nu)(1+\beta^2) + \beta^2\cot^2(\theta)\right]u_\theta \\ +\cot(\theta)\left[(2-\nu+\cot^2(\theta))\beta^2 - (1+\nu)\right]u \\ -\beta^2 w_{\theta\theta\theta\theta} - 2\beta^2\cot(\theta)w_{\theta\theta\theta} + \beta^2(1+\nu+\cot(\theta)^2)w_{\theta\theta} \\ -\beta^2\cot(\theta)(2-\nu+\cot(\theta)^2)w_\theta - 2(1+\nu)w \\ -\frac{a^2}{c_p^2}w_{tt} = 0 \ . \end{aligned} \tag{A.2}$$

Only the homogeneous form of the $w(\theta, t)$ equation needs to be considered since the external input $\underset{\sim}{p}_a(\theta, t)$ will be reduced to separated form. In addition the second order derivative acceleration terms will be ignored since these are immediately separated and may be conveniently returned after separating the R and θ terms.

The separated form of the dimensional dependent variables is

$$\begin{aligned} w(\theta, t) &= \sum_{n=0}^{\infty} P_n(\theta)w_n(t) \\ u(\theta, t) &= -\sum_{n=0}^{\infty} P_n^1(\theta)u_n(t) \ , \end{aligned} \tag{A.3}$$

where P_n is the $m = 0$ legendre polynomial and P_n^1 is the $m = 1$ form.

A.1 Preliminaries

Before separating these equations in the angle θ and time t some preliminary forms are used to make the algebra a little easier to follow.

The relationship between the $m = 0$ and $m = 1$ polynomial is

$$P_n^1(\theta) = P_{n\theta} \ . \tag{A.4}$$

Now the $m = 0$ legendre polynomial is P_n and it satisfies

$$P_{n\theta\theta} + \cot(\theta)P_{n\theta} + n(n+1)P_n = 0 \ , \tag{A.5}$$

while the $m = 1$ legendre polynomial P_n^1 satisfies

$$P_{n\theta\theta}^1 + \cot(\theta)P_{n\theta}^1 + n(n+1)P_n^1 - (1 + \cot^2(\theta))P_n^1 = 0 \ . \tag{A.6}$$

When the separated form of $w(\theta, t)$ and $u(\theta, t)$ are substituted to the shell equations it is necessary to reduce the higher derivatives of P_n and P_n^1 to become proportional to P_n. This is accomplished by differentiating the $m = 1$ form with respect to θ to obtain a relationship between the third and lower derivatives in θ.

Differentiating equation (A.6) and rearranging gives

$$\begin{aligned} P_{n\theta\theta\theta}^1 = \ & - \ \cot(\theta)P_{n\theta\theta}^1 + 2(1 + \cot(\theta)^2)P_{n\theta}^1 \\ & - \ n(n+1)P_{n\theta}^1 - 2\cot(\theta)(1 + \cot^2(\theta))P_n^1 \ . \end{aligned} \tag{A.7}$$

A.2 Separating $u(\theta, t)$ equation (A.1)

Since $w \propto P_n$ and $w_\theta \propto P_{n\theta} = P_n^1$ after substituting equation (A.3), equation (A.1) takes the form

$$\begin{aligned} & -\left(P_{n\theta\theta}^1 + \cot(\theta)P_{n\theta}^1 - \cot^2(\theta)P_n^1\right) u_n(t) \\ & -\frac{\beta^2}{1+\beta^2}\left(P_{n\theta\theta}^1 + \cot(\theta)P_{n\theta}^1 - \cot^2(\theta)P_n^1\right) w_n(t) \\ & +\nu P_n^1 u_n(t) + \left[\frac{1+\nu}{1+\beta^2} + \frac{\beta^2\nu}{1+\beta^2}\right] P_n^1 w_n(t) \\ & = -\frac{a^2}{(1+\beta^2)c_p^2} u_{ntt} = 0 \ . \end{aligned} \tag{A.8}$$

Substituting equation (A.6) into equation (A.8) becomes

$$\begin{aligned} &-\left[1-n(n+1)\right]P_n^1 u_n(t) \\ &-\frac{\beta^2}{1+\beta^2}\left[1-n(n+1)\right]P_n^1 w_n(t) \\ &+\nu P_n^1 u_n(t)+\left[\frac{1+\nu}{1+\beta^2}+\frac{\beta^2\nu}{1+\beta^2}\right]P_n^1 w_n(t) \\ &=-\frac{a^2}{(1+\beta^2)c_p^2}P_n^1 u_{ntt}=0\ , \end{aligned} \tag{A.9}$$

and rearranging, the coefficient of $P_n^1(t)$ yields the ordinary differential equation

$$\begin{aligned} &\left[1-\nu-n(n+1)\right] \quad u_n(t) \\ -\frac{1}{1+\beta^2}&\left[(n(n+1)-1+\nu)\beta^2+1+\nu\right] \quad w_n(t) \quad =\frac{a^2}{(1+\beta^2)c_p^2}u_{ntt}\ . \end{aligned} \tag{A.10}$$

A.3 Separating $w(\theta,t)$ equation (A.2)

This equation is somewhat more complicated than equation (A.2) due to the presence of a fourth derivative. There are two sets of terms in equation (A.2): the $u(\theta,t)$ terms and the $w(\theta,t)$ terms.

A.3.1 The $u(\theta,t)$ terms.

Consideration of equation (A.2) shows that the $u(\theta,t)$ terms are in two parts those without β^2 and those with β^2

1. *Terms not multiplied by β^2.*

   These terms are

   $$-(1+\nu)u_\theta-\cot(\theta)(1+\nu)u\ , \tag{A.11}$$

   and applying equation (A.3) this is

   $$(1+\nu)\left[P_{n\theta}^1+\cot(\theta)P_n^1\right]u_n(t)\ . \tag{A.12}$$

   If this is further written in terms of the zeroth legendre polynomial via equation (A.4) yields

   $$(1+\nu)\left[P_{n\theta\theta}+\cot(\theta)P_{n\theta}\right]u_n(t)\ , \tag{A.13}$$

and applying equation (A.5) this last form simplifies to

$$-(1+\nu)n(n+1)P_n u_n(t) \ . \tag{A.14}$$

2. *Terms multiplied by* β^2.

These terms are

$$u_{\theta\theta\theta} + 2\cot(\theta)u_{\theta\theta} - \left[1+\nu+\cot^2(\theta)\right]u_\theta + \cot(\theta)\left[2-\nu+\cot^2(\theta)\right]u \ , \tag{A.15}$$

and applying equation (A.3)

$$\begin{aligned} P^1_{n\theta\theta\theta} + 2\cot(\theta)P^1_{n\theta\theta} - \left[1+\nu+\cot^2(\theta)\right]P^1_{n\theta} \\ + \cot(\theta)\left[2-\nu+\cot^2(\theta)\right]P^1_n \ , \end{aligned} \tag{A.16}$$

where a multiplicative factor of $-u_n(t)$ has been dropped to simplify what follows.

From equation (A.7) replacing $P^1_{n\theta\theta\theta}$

$$\begin{aligned} -\cot(\theta)P^1_{n\theta\theta} + \left[2(1+\cot^2(\theta)) - n(n+1)\right]P^1_{n\theta} \\ -2\cot(\theta)(1+\cot^2(\theta))P^1_n + 2\cot(\theta)P^1_{n\theta\theta} \\ - \left[1+\nu+\cot^2(\theta)\right]P^1_{n\theta} + \cot(\theta)\left[2-\nu+\cot^2(\theta)\right]P^1_n \ , \end{aligned} \tag{A.17}$$

and simplifying yields

$$\cot(\theta)P^1_{n\theta\theta} + \left[1+\cot^2(\theta)-\nu-n(n+1)\right]P^1_{n\theta} - \left[\cot^3(\theta)+\nu\cot(\theta)\right]P^1_n \tag{A.18}$$

noting that this last term is multiplied by $-u_n(t)$.

Continuing similarly from equation (A.6) replacing $P^1_{n\theta\theta}$ gives

$$\begin{aligned} \cot(\theta)\left[-\cot(\theta)P^1_{n\theta} - n(n+1)P^1_n + (1+\cot^2(\theta))P^1_n\right] + \\ \left[1+\cot^2(\theta)-\nu-n(n+1)\right]P^1_{n\theta} - \left[\cot^3(\theta)+\nu\cot(\theta)\right]P^1_n \ , \end{aligned} \tag{A.19}$$

and simplifying

$$(1-n(n+1)-\nu)\left(P^1_{n\theta} + \cot(\theta)P^1_n\right) \ . \tag{A.20}$$

From equation (A.4)

$$P^1_{n\theta} + \cot(\theta)P^1_n = P_{n\theta\theta} + \cot(\theta)P_{n\theta} \ . \tag{A.21}$$

Substituting from equation (A.6) to the right-hand-side of equation (A.21) yields the simplified form

$$P_{n\theta\theta} + \cot(\theta)P_{n\theta} = -n(n+1)P_n \ , \tag{A.22}$$

and finally equation (A.20) with equation (A.22) yields

$$\left[1 - n(n+1) - \nu\right](-n(n+1)P_n) \ . \tag{A.23}$$

Returning the factor $-u_n(t)$ and the terms multiplied by β^2 are then

$$\beta^2\left[1 - n(n+1) - \nu\right]n(n+1)P_n u_n(t) \ . \tag{A.24}$$

3. *Combining both sets of terms.* Combining both sets of terms multiplying $u(t)$ gives

$$\Big[\beta^2(1 - n(n+1) - \nu) - (1+\nu)\Big]\, n(n+1)P_n u_n(t) \ . \tag{A.25}$$

A.3.2 The $w(\theta, t)$ terms.

These terms from equation (A.2) are

$$\begin{aligned} -\beta^2 w_{\theta\theta\theta\theta} - 2\beta^2\cot(\theta)w_{\theta\theta\theta} + \beta^2(1+\nu+\cot(\theta)^2)w_{\theta\theta} \\ -\beta^2\cot(\theta)(2-\nu+\cot(\theta)^2)w_\theta - 2(1+\nu)w \ . \end{aligned} \tag{A.26}$$

Applying equations (A.3) and (A.4) and dropping the factor $w_n(t)$ for convenience

$$\begin{aligned} -\beta^2 P^1_{n\theta\theta\theta} - 2\beta^2\cot(\theta)P^1_{n\theta\theta} + \beta^2(1+\nu+\cot(\theta)^2)P^1_{n\theta} \\ -\beta^2\cot(\theta)(2-\nu+\cot(\theta)^2)P^1_n - 2(1+\nu)P_n \ . \end{aligned} \tag{A.27}$$

Rearranging slightly yields

$$\begin{aligned} -\beta^2\left(P^1_{n\theta\theta\theta} + 2\cot(\theta)P^1_{n\theta\theta} - (1+\nu+\cot(\theta)^2)P^1_{n\theta} + \cot(\theta)(2-\nu+\cot(\theta)^2)P^1_n\right) \\ -2(1+\nu)P_n \ . \end{aligned} \tag{A.28}$$

The terms multiplying β^2 collectively are identical to that in equation (A.16) which leads to equation (A.23) and this gives the final result after slight rearrangement

$$\Big(\beta^2 n(n+1)\left(1 - n(n+1) - \nu\right) - 2(1+\nu)\Big)\, P_n w_n(t) \ . \tag{A.29}$$

A.3.3 Combining the $u(\theta,t)$ and $w(\theta,t)$ terms.

Combining the results in equations (A.25) and (A.29) yields

$$\begin{aligned}&\left[\beta^2(1-n(n+1)-\nu)-(1+\nu)\right]n(n+1)P_n u_n(t)\\ &+\left(\beta^2 n(n+1)\left(1-n(n+1)-\nu\right)-2(1+\nu)\right)P_n w_n(t)\ .\end{aligned}\tag{A.30}$$

A.4 Final Separated Forms

The final separated form of the homogeneous verions of the shell equations (A.1) and (A.2) is respectively

$$\begin{aligned}\left[1-\nu-n(n+1)\right]u_n(t)+\frac{1}{1+\beta^2}\left[(n(n+1)-1+\nu)\beta^2+1+\nu\right]w_n(t)\\ -\frac{a^2}{(1+\beta^2)c_p^2}\ddot{u}_n(t)=0\ ,\end{aligned}\tag{A.31}$$

and

$$\begin{aligned}\left[-(1+\nu)n(n+1)+\beta^2(1-n(n+1)-\nu)n(n+1)\right]u_n(t)\\ -\beta^2 n(n+1)\left[1-n(n+1)-\nu\right]w_n(t)\\ +2(1+\nu)w_n(t)+\frac{a^2}{c_p^2}\ddot{w}_n(t)=0\ ,\end{aligned}\tag{A.32}$$

and the shell movements are defined in equation (A.3).

Appendix B

Development of $(zi'_n(z))'$

The following is a development of the result

$$(zi'_n)' = \left(z + \frac{n^2}{z}\right) i_n - i_{n+1} \ , \tag{B.1}$$

noting the functional dependence if $i_n(z)$ upon z is assumed for notational clarity.

The approach used here to prove equation (B.1) starts from the two recurrence relations

$$i_{n-1} - in + 1 = \frac{2n+1}{z} i_n \ , \tag{B.2}$$

$$i'_n = i_{n+1} + \frac{n}{z} i_n \ . \tag{B.3}$$

From equation (B.3)

$$zi'_n = zi_{n+1} + ni_n \ , \tag{B.4}$$

and differentiating

$$(zi'_n)' = (zi_{n+1})' + ni'_n \ , \tag{B.5}$$

and substituting i'_n from equation (B.3)

$$(zi'_n)' = (zi_{n+1})' + ni_{n+1} + \frac{n^2}{z} i_n \ . \tag{B.6}$$

Applying the product rule to the first term on the right-hand-side of equation (B.6)

$$(zi_{n+1})' = i_{n+1} + zi'_{n+1} \ . \tag{B.7}$$

Referring to equation (B.3), multiplying by z and shifting indices from $n \to n+1$ yields a form for zi'_{n+1} which upon substitution to equation (B.7)

$$(zi_{n+1})' = i_{n+1} + z\left(i_{n+2} + \frac{n+1}{z} i_{n+1}\right) \ , \tag{B.8}$$

which simplifies to

$$(zi_{n+1})' = zi_{n+2} + (n+2)i_{n+1} \ . \tag{B.9}$$

This last result is substituted to the right-hand-side of equation (B.6) and gives

$$\begin{aligned} (zi'_n)' &= zi_{n+2} + (n+2)i_{n+1} + ni_{n+1} + \frac{n^2}{z} i_n \\ &= zi_{n+2} + 2(n+1)i_{n+1} + \frac{n^2}{z} i_n \ . \end{aligned} \tag{B.10}$$

The term i_{n+2} is eliminated by appealing to equation (B.2) from which

$$\begin{aligned} zi_{n-1} - zi_{n+1} &= (2n+1)i_n \ , \\ zi_{n+1} &= zi_{n-1} - (2n+1)i_n \ , \\ zi_{n+2} &= zi_n - (2n+3)i_{n+1} \ , \end{aligned} \tag{B.11}$$

and replacing zi_{n+2} from equation (B.11) in equation (B.10) gives

$$\begin{aligned} (zi'_n)' &= zi_n - (2n+3)i_{n+1} + 2(n+1)i_{n+1} + \frac{n^2}{z} i_n \\ &= zi_n - i_{n+1} + \frac{n^2}{z} i_n \\ &= \left(z + \frac{n^2}{z} \right) i_n - i_{n+1} \ , \end{aligned} \tag{B.12}$$

where equation (B.12) is the desired result.